THE GEOLOGICAL SOCIETY OF AMERICA®

Formation of waterfalls by intermittent burial of active faults

Luca C. Malatesta[†] **and Michael P. Lamb**
Division of Geological and Planetary Sciences, California Institute of Technology, 1200 East California Boulevard, Pasadena, California 91125, USA

ABSTRACT

Waterfalls commonly exist near bounding faults of mountain ranges, where erosional bedrock catchments transition to depositional alluvial fans. We hypothesize that aggradation on alluvial fans can bury active faults, and that the faults accumulate slip in the subsurface to produce a bedrock scarp. Following entrenchment of the alluvial fan, the scarp can be exposed as a waterfall. To explore this hypothesis, we derived a geometric model for waterfall height that depends on alluvial fan length and the relative time scales of (1) tectonic uplift, (2) a forcing mechanism for cycles of fan aggradation and incision, and (3) a response of fan aggradation to changes in sediment flux. We find that the model is consistent with observations at Gower Gulch, Death Valley, California, where a man-made drainage capture event in 1941 caused rapid fan incision and exposed a waterfall at the canyon-fan transition. We also compared the model to 62 waterfalls in 18 catchments of the Death Valley area and found that at least 15 of the waterfalls are best explained by the fault-burial mechanism. Using field measurements of grain size and channel geometries, we show that the fault-burial mechanism can produce the observed waterfall heights, measuring 4–19 m, under a uniform climatic forcing scenario requiring variations of 20% in precipitation during the late Pleistocene. The fault-burial mechanism, through the creation of upstream propagating waterfalls, may allow catchment-fan systems to experience frequent cycles of enhanced erosion in catchments and deposition on fans that likely convolve tectonic and climatic signals.

INTRODUCTION AND MOTIVATION

Waterfalls and steep bedrock steps are important components of mountain river systems, and they can serve as an agent to transfer tectonic, climatic, or autogenic signals upstream through a catchment (e.g., Howard, 1994; Clark et al., 2005; Wobus et al., 2006; Berlin and Anderson, 2007; Whipple et al., 2013; DiBiase et al., 2014). Retreating waterfalls and steps can produce fluvial terraces that are important landforms in tectonic and climatic reconstructions (Crosby and Whipple, 2006; Finnegan and Balco, 2013; DiBiase et al., 2014). Their migration forces a pulse of erosion by lowering the local base level of the adjacent hillslopes, which temporarily increases sediment delivery to the fluvial system (Humphrey and Heller, 1995; Carretier and Lucazeau, 2005; Gallen et al., 2011; Attal et al., 2015).

Several mechanisms and origins have been proposed to account for the formation of waterfalls in specific conditions. Relative eustatic forcing of sea cliffs results in knickpoints and waterfalls (Hayakawa and Matsukura, 2003; Bishop et al., 2005; Mackey et al., 2014). Large slumps can initiate waterfalls (Lamb et al., 2007). Preexisting topography of deep glacial valleys with vertical walls results in spectacular waterfalls. Differential incision rates between trunk stream and tributary can also create waterfalls at their confluence (Hayakawa and Matsukura, 2003). Cutoffs in bedrock meanders are another way to produce waterfalls within a river system (K.N. Johnson and N.J. Finnegan, 2017, personal commun.). Seismic slip with large throw can create waterfalls, like along the Tachia River in Taiwan following the 1999 M_w 7.6 Chi-Chi earthquake (Chen et al., 2002; Lee et al., 2005; Huang et al., 2013; Cook et al., 2013). Climatic forcing can also lead to the widespread creation of waterfalls (Crosby and Whipple, 2006). Waterfalls can develop at lithological boundaries with great changes in erodibility (Cook et al., 2009) and in vertically bedded substrates (Frankel et al., 2007). Finally, steepening of bedrock reaches and the coalescence of small steps in bedrock river channels form autogenic waterfalls in upstream reaches (Sklar and Dietrich, 2004; Chatanantavet and Parker, 2009; Whipple et al., 2013).

Despite this extensive work on the creation of waterfalls, many waterfalls exist without a clear formation mechanism. For example, significant waterfalls are common near the outlet of fault-bounded mountain catchments in the Death Valley area in the southwest United States (Fig. 1; this study). Many of these waterfalls have heights too large to be explained by coseismic throw, and no clear lithological controls can account for their location. To help explain these anomalous waterfalls—building off ideas of Humphrey and Heller (1995), Carretier and Lucazeau (2005), and Pepin et al. (2010)—Finnegan and Balco (2013) recently proposed a new mechanism to account for large waterfalls in the lower reaches of a catchment: burial of a fault by the aggradation of an alluvial fan immediately downstream of an active dip-slip fault. This raises the relative base level of the catchment, and tectonic slip can accumulate to that new level. If the fan incises again, it then exposes a waterfall that can retreat upstream. We call it the fault-burial mechanism. Transport-limited rivers flowing on alluvial fans are sensitive to environmental changes. Their bed slope scales inversely with water discharge and scales positively with the ratio of sediment flux over water discharge (Gilbert and Murphy, 1914; Mackin, 1948; Hooke, 1968; Schumm, 1973; Leopold and Bull, 1979). In particular, an increase in the ratio of sediment supply to water discharge, Q_s/Q_w, is thought to cause an increase in the channel-bed slope on the alluvial fan and result in fan aggradation, whereas a decrease in Q_s/Q_w should drive fan entrenchment (Wells and Harvey, 1987; Harvey et al., 1999; DeLong et al., 2008; Rohais et al., 2012). In addition, climatic changes can affect channel-bed slopes through changes in sediment grain sizes, D, that are supplied to channels from hillsides and by different competencies of the higher-discharge flows (Lane, 1937; Leopold

[†]Present address: Department of Earth & Planetary Sciences, University of California Santa Cruz, 1154 High Street, Santa Cruz, California 95064, USA; lcmalate@ucsc.edu.

GSA Bulletin; https://doi.org/10.1130/B31743.1; 11 figures; 2 tables; Data Repository item 2017320.

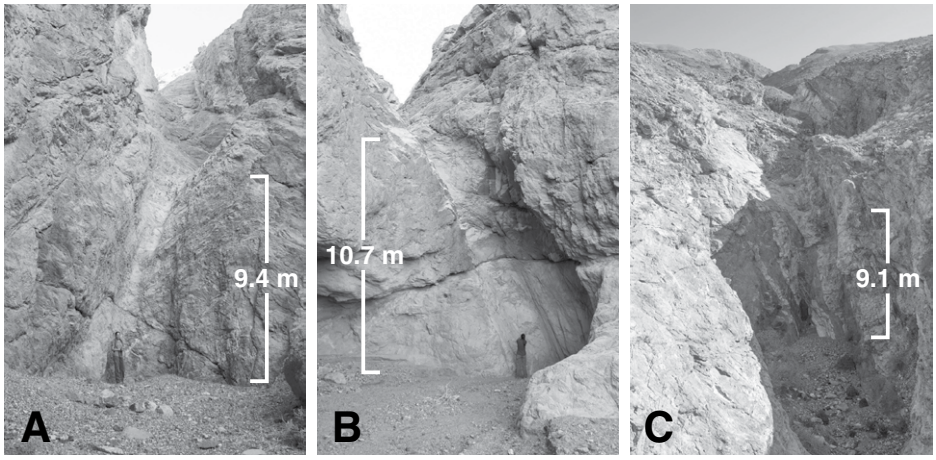

Figure 1. Field examples of waterfalls lying very close to the fan apex: in Death Valley's Black Mountains: (A) Badwater and (B) South Badwater 4; in Panamint Valley's eponymous mountains: (C) South Park Canyon. See Figure 4 for locations.

and Maddock, 1953; Paola et al., 1992; D'Arcy et al., 2016). This makes alluvial fans very dynamic landforms that can regularly aggrade and incise because of climatic forcing (e.g., Poisson and Avouac, 2004; D'Arcy et al., 2014) or autogenic processes (e.g., Carretier and Lucazeau, 2005; Nicholas and Quine, 2007; van Dijk et al., 2009; Reitz and Jerolmack, 2012). The fault-burial mechanism, which was also proposed by DiBiase et al. (2014) for the San Gabriel Mountains, has the potential to explain waterfalls in the Death Valley area and many more sites. This mechanism has not yet been tested with a model or focused field work.

In this study, we tested if the intermittent burial of active dip-slip fault scarps by cyclically aggrading and incising alluvial fans is a valid mechanism to create waterfalls at the base of catchments. First, we formalized mathematically the geometry of the fault-burial mechanism and used empirical laws to link waterfall heights with changes in water discharge that control fan slopes. Second, we took advantage of the engineered Gower Gulch catchment in Death Valley to test the relationship between waterfall height and water discharge variations in a controlled field site. Third, we applied the hypothesis to unexplained waterfalls of the Death Valley area. There, we compared the change in precipitation required for the aggradation and incision of the alluvial fans, which buries and exposes scarps as high as the surveyed waterfalls, to the regional climatic record of late Pleistocene wet and dry episodes.

MODEL FOR WATERFALL GENERATION

Of the many landscapes that combine active faults and alluviation, we chose to conceptualize the fault-burial mechanism in coupled catchment-fan systems. Coupled catchment-fan systems are small, self-contained, complete sediment-routing systems that are well studied as elemental landscapes to understand the fundamental dynamics ruling larger systems (Allen and Densmore, 2000; Densmore et al., 2007; Rohais et al., 2012). They can be summarized as the combination of a catchment draining an uplifting block and a basin in relative subsidence, where the sediments eroded from the catchment are entirely captured and form an alluvial fan. It has been argued that the evolution of downstream fans can influence upstream dynamics by varying the base level of the upstream catchment at a relatively high frequency (Humphrey and Heller, 1995; Carretier and Lucazeau, 2005; Pepin et al., 2010).

Here, we investigated the mechanism of waterfall formation by fault burial as simply as possible using a one-dimensional (1-D) model for the long-profile evolution of a catchment-fan system. In this conceptual model, a vertical dip-slip fault separates the uplifting and subsiding domains. We did not address channels dominated by debris flows. Elevation is fixed relative to base level, and uplift U is uniform in the uplifting reach. Intermittent burial of the fault scarp is driven through aggradation on the fan driven by changes in alluvial riverbed slope. Alluvial rivers can change their bed slope in response to changes in subsidence, grain size, channel width, water discharge, Q_w, and sediment supply, Q_s (Lane, 1937, 1955; Leopold and Maddock, 1953; Knox, 1975; Bull, 1991). On small alluvial fans, channel slopes vary with changes in these parameters but tend to remain only lightly concave up or linear across the fan (Bull, 1964; Densmore et al., 2007; Stock et al., 2008). Here, we modeled fan slopes as linear for simplicity, following Allen and Densmore (2000).

Consider the simple geometry where the alluvial channel on the fan alternates between two linear slopes, which have the same horizontal length and which hinge on the same base level, so that the channel always ends at the same point (Fig. 2). This type of fan geometry occurs, for example, if there is an important valley channel along the toe of the fan that removes sediment there, or if fan aggradation is balanced by subsidence so that the toe of the fan is fixed (Hooke, 1968; Whipple and Trayler, 1996). A forcing time scale, which could be allogenic or autogenic, would pace the alternation between steep and gentle channel configurations. A transition from gentle-slope (Fig. 2A) to steep-slope (Fig. 2B) configuration results in channel aggradation, which drives alluvial backfilling upstream of the fault scarp, burying the bedrock scarp (e.g., Frankel et al., 2015). Erosion of the bedrock scarp at the canyon-fan transition stops as long as it is shielded under alluvium. The elevation of the now-buried bedrock bed immediately upstream of the scarp increases with repeated earthquakes, thinning the alluvial cover until bedrock is again exposed in the riverbed at the scarp (Fig. 2C). Once bedrock is again exposed at the scarp, throw cannot accumulate anymore. The offset of any new earthquake will be transmitted upstream by scarp retreat. When the channel on the fan transitions back to the gentle slope configuration, the exposed fault scarp forms a waterfall (Fig. 2D). The waterfall then retreats upstream to propagate the base-level fall through the catchment. The fault-burial mechanism allows tectonic slip to accumulate over several seismic cycles and results in waterfall heights that can be multiple times larger than coseismic throw.

In this simple scenario, the maximum height of the scarp, h_{max}, is the product of the difference between steep and gentle equilibrium alluvial-bed slopes, $\Delta S = S_{steep} - S_{gentle}$, and the length of the fan, L_{fan}, or:

$$h_{max} = \Delta S\, L_{fan}. \quad (1)$$

To model channels with radial profiles departing strongly from the linear slope assumption, Equation 1 would need to be adjusted. Equation 1 defines a maximum exposed scarp height because the time scale of forcing, t_f, during which the fan channel is in a steep-slope configuration might be shorter than what is needed for the uplifting bedrock scarp to grow to its full potential h_{max}. The waterfall height can also be limited because a fan may adjust slowly in response to allogenic forcing (e.g., climate), and its channel

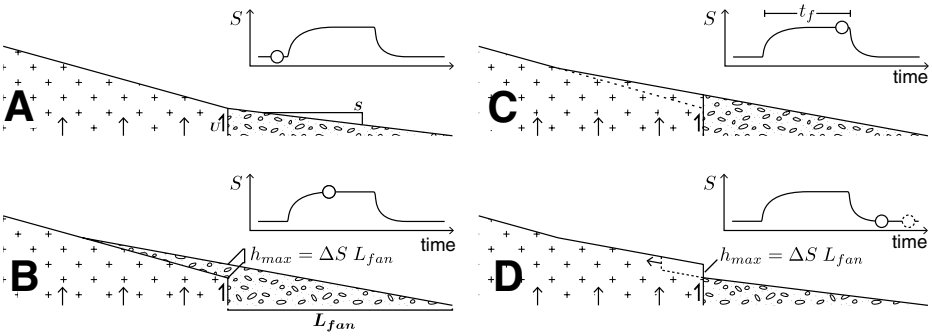

Figure 2. Illustration of the fault-burial mechanism in regime I: a river flows from an uplifting bedrock block (left) onto an alluvial fan (right). The inset plots show the evolution of the alluvial equilibrium local slope, S, over time as the system is disturbed by a phase of aggradation followed by a return to initial conditions. (A) At equilibrium, the alluvial fan grades into the bedrock channel at the scarp, where a break in slope reflects the change from detachment-limited to transport-limited equilibriums. (B) A change in equilibrium slope forces aggradation of the fan, and the bedrock channel backfills, effectively shielding it from fluvial erosion until the alluvium is stripped. The maximum height of the future waterfall (h_{max}) is set by the thickness of alluvium above the scarp. (C) Uplift (U) brings the entire bedrock reach to the surface during the shielding period. (D) When the fan incises to return to its initial gentle slope, it exposes a waterfall at the location of the scarp. The tectonic displacement thus accumulated is released at once and retreats upstream in the drainage (dashed profile). Here, t_f is time scale of forcing, and L_{fan} is the length of the fan.

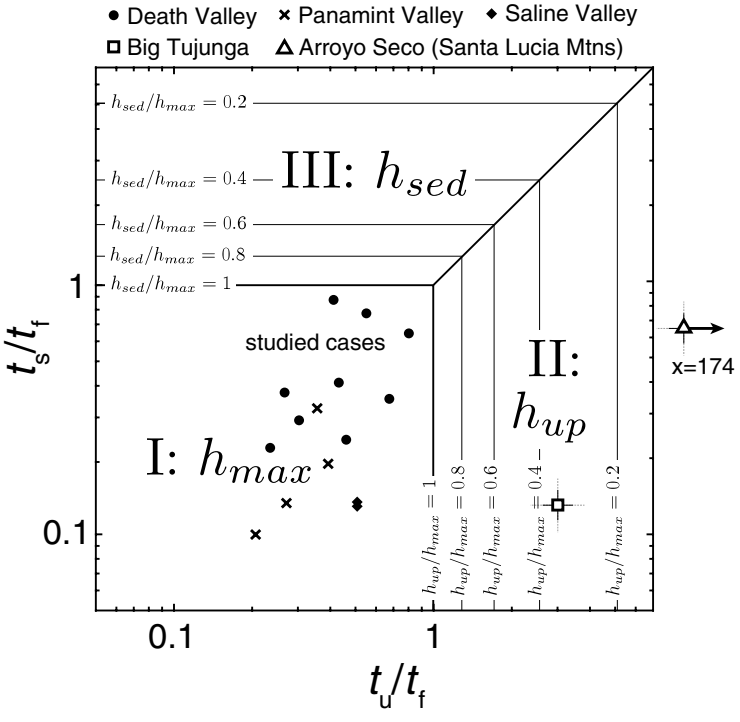

Figure 3. Three time-scale regimes determine the effective height of the scarp: regime I determines maximal height h_{max}, regime II determines the total uplift reached during the shielding period, h_{up}, and regime III determines the thickness of sediment aggradation, h_{sed}, at the scarp. The regimes depend on the relative durations of the forcing, sedimentary, and uplift time scales (t_f, t_s, and t_u, respectively). The contour lines mark waterfall heights normalized by h_{max}. The relative time scales of the sites in Saline, Panamint, and Death Valleys are indicated with circles, crosses, and diamonds, respectively.

may not reach its equilibrium steep transport slope within the forcing time scale. These scenarios highlight three important time scales for determining the height of scarps created by this mechanism. (1) The forcing time scale, t_f, sets how long the fan stays in a steep equilibrium geometry, and it is determined by external forcing like climate change or internal catchment-fan dynamics like a mass wasting event. (2) The uplift time scale, t_u, is the time it takes for the fault scarp to be uplifted to the elevation of the new base level. The uplift time scale is simply the maximal height of aggradation at the scarp divided by the uplift rate:

$$t_u = \frac{h_{max}}{U}. \quad (2)$$

Finally, (3) the sedimentary time scale, t_s, determines how long it takes for the alluvial channel to aggrade to the new higher elevation at the scarp, where t_s is a function of the volume (V) of the reach in the new geometry and of the coarse sediment flux from the catchment necessary to fill this volume, which is the product of the coarse fraction of the total flux, f_{coarse}, erosion rate, E, and drainage area, A. However, the pattern and rate of sediment deposition on the fan depend on changes in channel width, flood hydrograph, pattern of tectonic accommodation, initial grain-size composition, and downstream fining, so that in general:

$$t_s \leq \frac{V}{f_{coarse} EA}. \quad (3)$$

The relative durations of t_f, t_u, and t_s define three regimes of waterfall heights (Fig. 3). In regime I, the forcing time scale is the longest ($t_f > t_u$ and $t_f > t_s$), the scarp has enough time to aggrade and steepen to the new base level, and the scarp height reaches its maximum value given by Equation 1 (as is the case in Fig. 2). In regime II, the uplift time scale is the longest ($t_u > t_f$ and $t_u > t_s$), the scarp does not grow fast enough to reach the new base level before the alluvial channel incises again, and the scarp height is limited to

$$h_{up} = U\, t_f = h_{max}\left(\frac{t_u}{t_f}\right)^{-1}. \quad (4)$$

In regime III, the sedimentary time scale is the longest ($t_s > t_f$ and $t_s > t_u$), and the alluvial aggradation rate at the scarp limits the growth of the future waterfall to h_{sed}, which is the total alluvial thickness gained at the scarp at the end of the forcing period. Regime III does not have an analytical solution for scarp height because it requires modeling changes in river profile through time. However, by inspection of Figure 3, we

see that regimes II and III share a common boundary, where $t_u = t_f$. Uplift and sediment-limited heights must be conformable along this boundary so that

$$h_{sed} = h_{max}\left(\frac{t_s}{t_f}\right)^{-1}. \quad (5)$$

We normalize Equations 4 and 5 by h_{max} to obtain three nondimensional formulas that are functions of the axes of the regime plot shown in Figure 3.

MODEL APPLICATION TO EXTERNAL FORCING

The conceptual model we put forward can be explored in field cases where simple fan-catchment systems contain large unexplained waterfalls. After establishing the time scales t_f, t_u, and t_s, the model regime can be determined and the expected waterfall height defined.

The waterfall height in regime I is set by the change in channel slope, ΔS, and the length of the fan, L_{fan} (Eq. 1). L_{fan} can be measured on maps and satellite images. ΔS can be measured if the fan is presently at the gentle equilibrium configuration, and the relict higher-gradient configuration is preserved in the fan morphology. Otherwise, the gentle slope is buried, and only the steep slope is observable in the field. In that case, the gentle slope can be deduced with hydraulic resistance equations under the assumption of constant bankfull Shields stress (Paola et al., 1992) as described below.

The geometry of a transport-limited alluvial channel is largely set by the hydraulic parameters of water discharge and sediment transport capacity, as well as the sediment grain size (Parker, 1978). Conversely, we can retrieve hydraulic parameters from surveyed channel geometries using empirical equations. Water discharge, Q_w, can be evaluated following conservation of mass from cross-section-averaged flow velocity, u, bankfull water depth, h_{bf}, and the computed width, w_r, obtained by dividing the surveyed cross-section area by h_{bf}:

$$Q_w = u\, h_{bf} w_r. \quad (6)$$

Flow velocity, in turn, can be estimated using a version of the Manning-Strickler relation for the resistance of steady uniform flow as formulated by Parker (1991):

$$\frac{u}{u_*} = 8.1\left(\frac{h_{bf}}{k_s}\right)^{1/6}, \quad (7)$$

in which u_* is the bed shear velocity equal to $\sqrt{gR_hS}$, R_h is the hydraulic radius, and k_s is the bed roughness length scale equal to twice the D_{84} grain-size percentile. Bed-load sediment transport, Q_s, is determined by an empirical law (Meyer-Peter and Müller, 1948; Wong and Parker, 2006):

$$\frac{Q_s}{(RgD^3)^{1/2}} = 4.6W(\tau_{*sf} - \tau_{*c})^{8/5}, \quad (8)$$

where R is the submerged density of the sediment, W is the width of the channel from bank to bank, τ_{*sf} is the skin friction component of bankfull Shields number τ_{*T}, and $\tau_{*c}(S)$ is the slope-dependent critical Shields number (Lamb et al., 2008). Most self-formed alluvial rivers tend toward a certain value of the Shields stress at bankfull, which depends on the bed grain size (e.g., Paola et al., 1992; Parker et al., 2007; Trampush et al., 2014). The total bankfull Shields stress is partitioned between that due to skin friction and that due to morphological form drag stress: $\tau_{*T} = \tau_{*sf} + \tau_{*m}$ (Einstein and Barbarossa, 1952). The Shields number for morphologic form drag, τ_{*m}, accounts for the channel's form, bed form, and banks, and the skin friction component, τ_{*sf}, drives sediment transport. We use $f_{skin} = \tau_{*sf}/\tau_{*T}$ to denote the proportion of skin friction in τ_{*T}. For steady and uniform flow, the total bankfull Shields stress can be written as

$$\tau_{*T} = \frac{R_h S}{RD}. \quad (9)$$

Following Parker et al. (1998), we combine Equations 6 and 7 and solve them for h_{bf}; we then insert the latter in the combination of Equations 8 and 9, where $R_h = f_{radius} \times h_{bf}$ with $f_{radius} = \frac{R_h}{h_{bf}}$ and finally solve for S to obtain an equation for the equilibrium slope as a function of sediment and water fluxes:

$$S = \left\{\left[\left(\frac{Q_s}{4.6W\sqrt{RgD^3}}\right)^{5/8} + \tau_{*C}(S)\right]\frac{RD}{f_{skin}f_{radius}}\left(\frac{8.1Wg^{1/2}}{Q_w k_s^{1/6}}\right)^{3/5}\right\}^{10/7}. \quad (10)$$

Equation 10 illustrates how alluvial slope is sensitive to changes in Q_w, Q_s, W, and D (Fig. 4). Equation 10 can be combined with Equation 1 to calculate the maximum waterfall height, h_{max}, for given environmental changes that produce a change in channel-bed slope. Depending on the relative magnitudes of time scales t_f, t_u, and t_s, the expected waterfall heights in the uplift- or sedimentation-limited regimes, h_{up} and h_{sed}, can then be found from Equations 4 and 5. On the other hand, if waterfall heights can be readily measured in the field, Equations 1 and 10 can be used to invert and solve for changes in one of the controlling parameters—Q_w, Q_s, W, or D—that are needed to produce a waterfall of a known height by the fault-burial mechanism. In the next section, we develop this idea further to invert waterfall heights for paleoriver discharge.

Inverting Waterfall Heights for Paleoriver Discharge

We cannot expect climate forcing to uniquely affect a single variable in a catchment-fan system. However, we argue that for small catchment-fan systems, it is reasonable to consider changes in water discharge as the first-order driver of channel slope variations on the

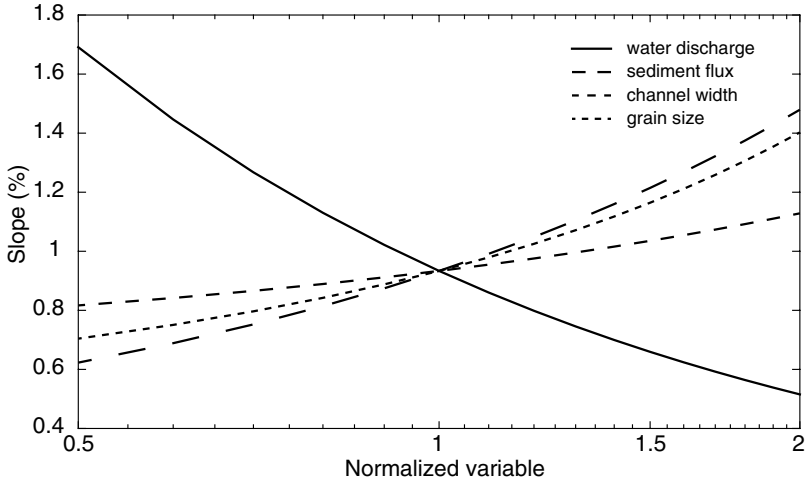

Figure 4. Effect of changes in water discharge (Q_w), sediment flux (Q_s), channel width (W), and grain size (D) on the equilibrium slope (S) of an alluvial river (Eq. 9). Each of the four parameters is individually changed from half to double its reference value on the x-axis. At , the reference values are Q_w = 1[m³/s], Q_s = 0.005[m³/s], W = 10[m], and D = 0.01[m].

alluvial fan while keeping other parameters, in particular Q_s, fixed. It is partly justified if the catchments are near topographic equilibrium, such that sediment supply is in balance with stable tectonic uplift over the period and region of interest, in this case, the late Pleistocene in the Death Valley area (Jayko, 2005; Lee et al., 2009; Frankel et al., 2015). Climate change might also induce variations in hillslope storage of sediment (Bull, 1991; Harvey et al., 1999; DeLong et al., 2008), but storage is expected to be small in steep, rapidly uplifting landscapes (Lamb et al., 2011) typical of the semiarid southwestern United States, where we apply the model. We nevertheless recognize that any change in sediment flux, grain size, and channel width is expected to scale positively with increased water discharge (Fig. 4). The effect would be to partly reduce the inferred change in channel slope, ΔS, caused by Q_w alone, which would lead to smaller waterfall height h_{max} by fault burial. Changes in riverbed slopes can also result from autogenic mechanisms (Nicholas and Quine, 2007; van Dijk et al., 2009; Reitz and Jerolmack, 2012), but the uniformity of the field sites we use—all are currently aggraded in or close to the steep geometry (as discussed in "Field Sites and Methods" section)—supports the argument of uniform external forcing. As we will show, our inferred water discharge changes inverted from measured waterfall heights are regionally consistent and are comparable to independent precipitation proxies.

Here, we show how measurements of waterfall height, along with other field measurements, can be used to infer paleoriver bankfull discharge. Assuming that the catchment is currently in a steep configuration, field observations give the modern channel-bed slope S_{steep}, channel width W, and median bed grain size, D. By rearranging Equations 6 and 7, the lower bankfull discharge for the steep configuration can be estimated from:

$$Q_{w\,Low} = 8.1W\left(\frac{\tau_* RD}{S_{steep}}\right)^{11/6}\frac{(gS_{steep})^{1/2}}{k_s^{1/3}}. \quad (11)$$

The higher bankfull water discharge can also be found from Equations 6 and 7, except in this case, the channel-bed slope S_{gentle} is inferred from the waterfall height from Equation 1, that is, $S_{gentle} = S_{steep} - (h_{max}/L_{fan})$. Thus, the high bankfull water discharge becomes

$$Q_{w\,High} = 8.1W\left(\frac{\tau_* RD}{S_{steep} - \frac{h_{max}}{L_{fan}}}\right)^{11/6}\frac{\left(g\left(S_{steep} - \frac{h_{max}}{L_{fan}}\right)\right)^{1/2}}{k_s^{1/3}}. \quad (12)$$

The two water discharge Equations 11 and 12 for the modern steep and reconstructed gentle geometries can be used in a ratio of discharges that directly reflects the magnitude of the change in bankfull discharge necessary to produce a waterfall of height h_{max} in regime I (Fig. 3), assuming that no other parameters change between the two configurations except bankfull water discharge:

$$\frac{Q_{w\,High}}{Q_{w\,Low}} = \left(1 - \frac{h_{max}}{S_{steep}L_{fan}}\right)^{-4/3}. \quad (13)$$

Equation 13 is a function of the three parameters S_{steep}, h_{max}, and L_{fan}, which can all be measured in the field and/or from remote-sensing data. To test the validity of the model, we verified Equation 13 with Gower Gulch, which experienced a known man-made change in drainage area that resulted in fan incision and exposed a waterfall. Next, we applied the model to reconstruct discharge changes during the Pleistocene based on surveyed waterfalls in the Death Valley area.

FIELD SITES AND METHODS

Field Sites

We applied the alluvial fault-burial mechanism to field sites in southern California (Fig. 5). The three locations—Saline, Panamint, and Death Valley—lie in the southwestern corner of the Basin and Range Province, where the normal faults of horsts and grabens are linked by strike-slip faults that reflect the dextral shear component of the Walker Lane (Frankel et al., 2008). We assumed that the late Pleistocene

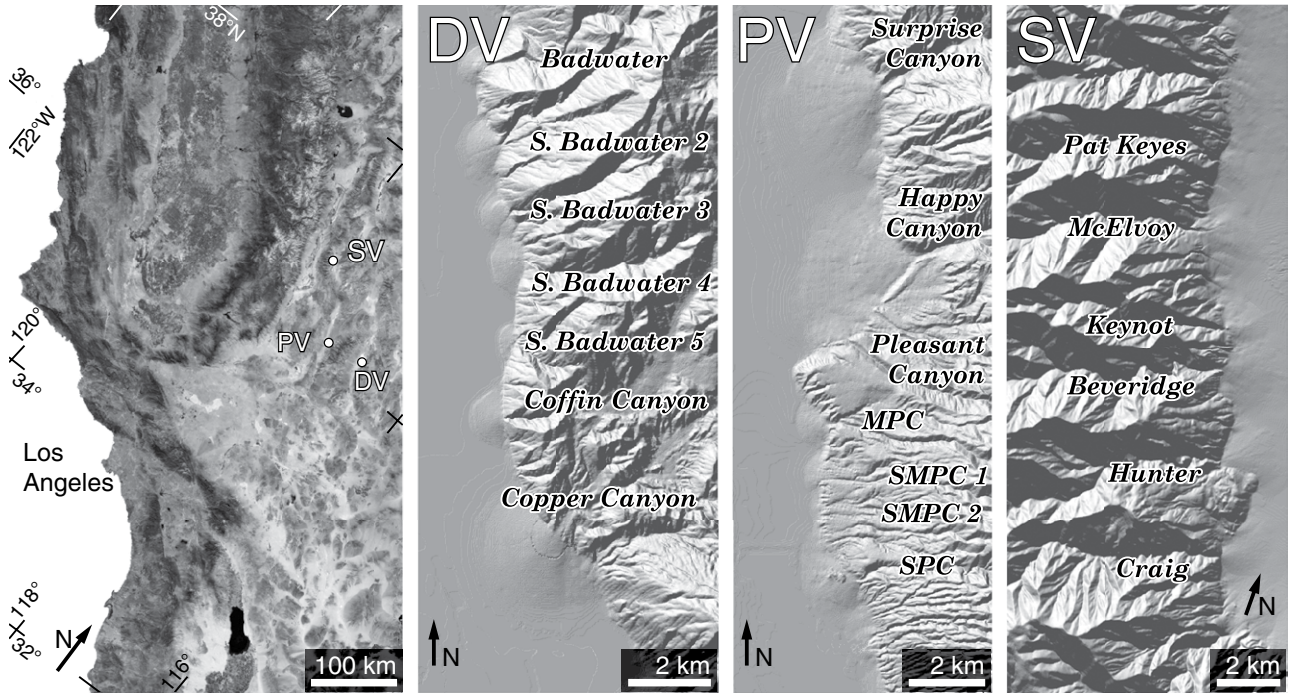

Figure 5. From left to right: Location map of the field sites in southern California, with Panamint Valley (PV), Saline Valley (SV), and Death Valley (DV) noted; Black Mountains in Death Valley; Panamint Mountains in Panamint Valley (MPC—Middle Park Canyon, SMPC1 and 2—South Middle Park Canyon 1 and 2, SPC—South Park Canyon); Inyo Mountains in Saline Valley.

climate evolved similarly in the three adjacent valleys, and that neighboring fans have faced similar changes in hydraulic forcing proportional to changes in precipitation (Horton, 1945; Freeze, 1974). In most of the catchments of these sites, waterfalls and very steep knickpoints interrupt the river profiles within 100 m of the alluvial-fan apex. These steps have several times the height of coseismic throw on the range-bounding fault (Fig. 1; Klinger and Piety, 2001; Frankel et al., 2015) and so cannot be explained as a result of single earthquakes.

In Saline Valley, the studied catchment-fan systems lie on the eastern slope of the Inyo Mountains and are separated from the valley floor by the normal and east-dipping Eastern Inyo fault (Fig. 5, SV). The fault marks the abrupt transition from the very steep catchments of the Inyo Mountains, culminating at 3384 m above sea level (masl) on Keynot Peak, to the flat valley floor (320 masl). The striking transition indicates that the Eastern Inyo fault has consistently ruptured along the same surface scarp in the recent geological past. Excellent thermochronological work constrains the exhumation of the Inyo Mountains at the level of Saline Valley and sets the throw rate of the fault at 0.4–0.7 mm/yr since 2.8 Ma (Lee et al., 2009).

The second field site, in Panamint Valley, includes the catchments flowing west of the Panamint Mountains and their respective alluvial fans (Fig. 5, PV). The Panamint Valley fault zone, normal and west dipping, separates the Panamint Mountains (topped by Telescope Peak, 3367 masl) from the floor of the eponymous valley (315 masl) and is connected to the Eastern Inyo fault by the right-lateral strike-slip Hunter Mountain fault (Burchfiel et al., 1987). Unlike the Eastern Inyo fault, the Panamint Valley fault zone has a complex surface expression with several successive splay faults separating the basin from the mountain. As a consequence, alluvial fans are often telescoped and abandoned by the changing location of the surface scarp (Numelin et al., 2007; Mason and Romans, 2015). Slip rate on the fault zone ranges from 0.1 to 2 mm/yr (Hart et al., 1989), with minimal slip rate of 0.34 mm/yr since 0.9 Ma

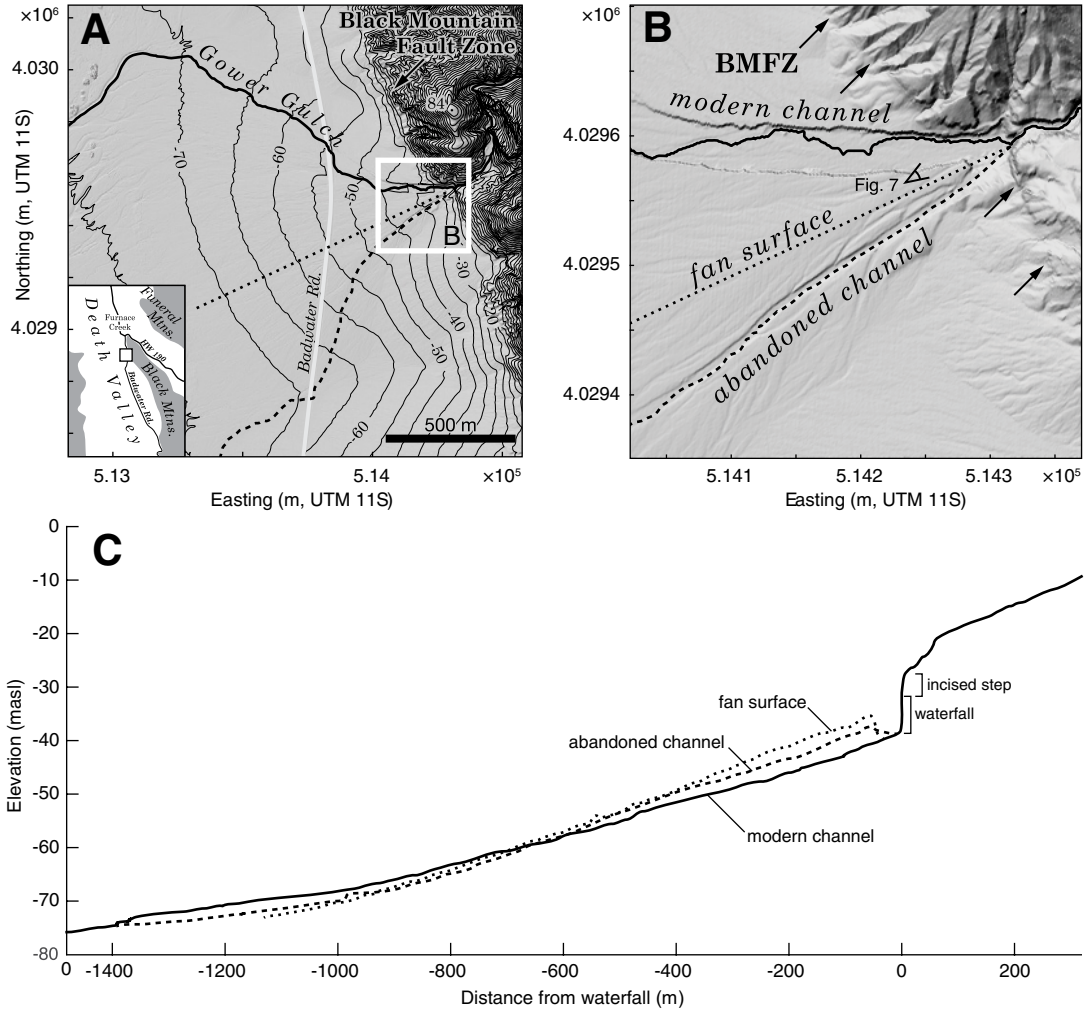

Figure 6. Maps and profiles of Gower Gulch extracted from the light detection and ranging (LiDAR) survey of Snyder and Kammer (2008). (A) Map of the alluvial fan at the outlet of Gower Gulch. The continuous black line marks the modern path of the Gower Gulch, and the dashed line is its abandoned course, while the dotted line indicates the trace of the fan profile. (B) Close-up of the fan apex, where arrows indicate the surface trace of the Black Mountain fault zone (BMFZ). (C) Longitudinal projected profiles of the fan surface, the abandoned channel, and the modern channel. The step at the apex is made of a vertical waterfall topped by an incised ledge that is not picked up by LiDAR (for detailed view, see Fig. 7; masl—m above sea level).

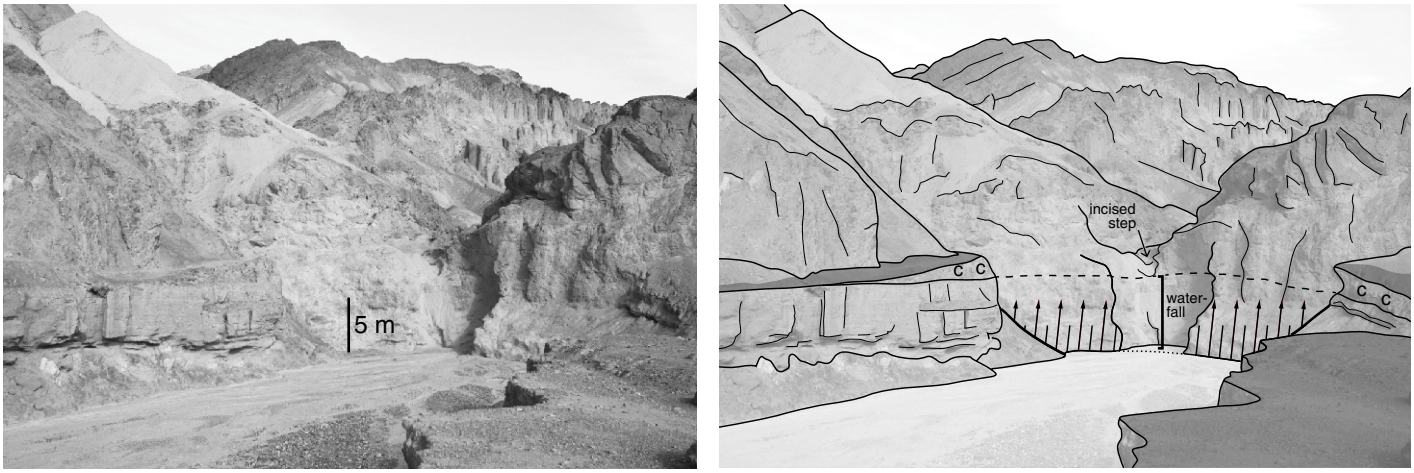

Figure 7. Apex of the Gower Gulch fan. Gower Gulch lies 20 km to the north of Badwater in Figure 4. To the right, the picture is completed with an interpretation sketch: the abandoned steep alluvial-fan surface is in medium gray, with dashed lines projecting its elevation onto the bedrock footwall, and the incised channel in light gray; C indicates colluvium that covers the abandoned alluvial-fan surface, and the upward arrows are the fault plane.

around Ballarat, next to our zone of study (Vogel et al., 2002).

The third field site lies along the Central Death Valley fault zone that runs at the foot of the Black Mountains, one valley east of the Panamint site (Fig. 5, DV). The configuration of the Black Mountain catchment-fan systems on the east flank of Central Death Valley is similar to Saline Valley with a well-defined single fault trace marking the boundary between the steep catchments of the Black Mountains, peaking at Dante's view (1699 masl), and the flat bottom floor (85 m below sea level), over which alluvial fans aggrade (Jennings, 1994). The west-dipping Black Mountain fault zone has a normal motion, and the Holocene slip rates are estimated between 1 and 3 mm/yr, with average coseismic throw around 2.5 m (Klinger and Piety, 2001).

In Death Valley, we additionally used the alluvial fan of Gower Gulch (4 km south of the junction between Highway 190 and Badwater Road, 36°24.6′N, 116°50.5′W; Fig. 6) as a controlled case study to test our hypothesis. In 1941, to protect settlements at Furnace Creek, the flows of the Furnace Creek catchment were diverted into the small mudstone catchment of Gower Gulch, effectively increasing its drainage area from 5.8 km^2 to 439 km^2 (Troxel, 1974; Dzurisin, 1975; Snyder and Kammer, 2008) and routing igneous and metamorphic cobbles from the Amargosa Range through the original mudstone catchment. As a result of the increased water discharge, the alluvial fan of the enlarged catchment dramatically incised. In 2014, a 6.75 m waterfall was exposed at its apex, where the extensional Death Valley fault zone bounds the mountain (Fig. 7). In 1974, Dzurisin (1975) measured 5.7 m of incision at the apex of the fan; 84% of the total incision was already completed in the 33 yr that followed the capture, and 16% occurred in the remaining 40 yr. The fast incision response of the alluvial channel in the decades that followed the capture suggests that the modern geometry is close to equilibrium.

The drainage areas of the studied catchments vary between 5 and 50 km^2 (see Table 1 for details), and they all share the same attributes of steep catchments (gaining on average 300 m for every horizontal kilometer) with a high relief (1500–2500 m). All the alluvial fans but one (McElvoy in Saline Valley) are barely incised. They are in a steep configuration corresponding to the contemporary interglacial aridity that followed the last pluvial maximum, when we would expect the fans to be incised by the greater water discharge.

The three sites experience a similar arid climate with a gradient in precipitation increasing with altitude from 0–4 cm/yr on the valley floor to 9–20 cm/yr at 1000 masl and above (Jayko, 2005). Rain is very infrequent, and several years of rainfall are often delivered during one intense short-lived event (Jayko, 2005). The recent climate history of the region saw increased aridity after the moisture high of the last pluvial maximum. At 20 ka, the region of Death Valley is estimated to have experienced about twice the amount of modern precipitation with an average temperature 5–6 °C cooler than today according to paleolake levels (Ku et al., 1998; Lowenstein et al., 1999; Menking et al., 2004), pollen (Thompson et al., 1999), and oxygen isotope records (Quade et al., 2003). To reconstruct a ratio for water discharges that explains all surveyed waterfalls created at different times in the late Pleistocene, we relied on the assumption that the late Pleistocene climatic cycles were similar.

Field Methods and Collected Data

We surveyed a total of 62 waterfalls in 18 catchments, listed in Table DR1.[1] We restricted the survey to the first three waterfalls within a few hundred meters upstream of the alluvial-fan apex to avoid falls that could have significantly changed height as they retreated or that could be due to coalescing steps during upstream propagation. Successive waterfalls in the same canyon would be the result of successive fault-burial events. The heights were measured from the surface of the plunge pool alluvium to the lip of the fall using a handheld laser range finder with 10 cm precision. In a few places, waterfalls and surrounding cliffs were impassable, limiting the survey to the first obstacle. Examples of surveyed waterfalls are shown in Figure 1.

We surveyed the geometry of the active channel at the fan apex in catchments selected for the analysis and a few other ones (Table 1). Sediment grain-size values are based on the median value of the second semi-axis of 100 grains measured every 0.5 m along a survey measuring tape stretched in the along-stream direction across bars and thalweg. At a few sites, only 50 grains were measured. The hydraulic radius R_h

[1]GSA Data Repository item 2017320, List of height, location and type of all 62 surveyed waterfalls, is available at http://www.geosociety.org/datarepository/2017 or by request to editing@geosociety.org.

TABLE 1. LIST OF HYDRAULIC PARAMETERS IN ALL THE SURVEYED CATCHMENTS IN SALINE, PANAMINT, AND DEATH VALLEYS

Catchment	Fan length (m)	Watershed area (km^2)	Channel width (m)	Slope (%)	D_{50} (mm)	D_{84} (mm)	τ^*	Rh
Gower Gulch active channel	1300	439	30	3.7	16†	59.5†	0.36	0.288
Gower Gulch old channel	1300	5.8	6.1	4.2	4.7†	9.9†	0.36§	0.073
Badwater	1770	5.2	9.2	13.1	18.7	41.9	0.28	0.071
S Badwater 3	850	3.9	6.5	8.9	7.4†	77.3†	0.31	0.047
S Badwater 4	950	6.1	4.8	7.3	5.2†	11.3†	0.38	0.049
S Badwater 5	560	1.9	13.6	8	4.7†	9.9†	0.43	0.046
Coffin Canyon	1000	11.1	6.4	7.9	9.3	22.6	0.40	0.085
Pleasant Canyon	2500	33	5.3	8.9	21	93	0.20	0.059
South Park Canyon	1250	8.3	6.8	11.7	19.3	58.1	0.34	0.146
Pat Keyes	1800	21.4	18.4	11	8.3	51.8	1.06	0.135
McElvoy	2300	23.3	11.6	10.3	44.4	157.1	–	–
Keynot	1500	10	19.3	15.3	29.2	142.3	–	–
Beveridge	2100	28.6	10.6	16.9	58	204	–	–
Hunter Canyon	2000	23.2	15.7	10.7	36	162.8	–	–
Craig Canyon	1700	22.6	14.4	9.5	60.5	275.1	–	–

Notes: Grain sizes were measured by picking about 100 clasts along a stream transect with 0.5 m spacing crossing thalweg and bars.
†Grain-size distributions based on less than 100 counts; Gower Gulch (GG) active = 55, GG old = 50, S Badwater (SB) 3 = 50, SB4 = 75, SB5 = 75 grain counts.
§Reconstructed value.

was calculated as the bankfull cross-sectional area of flow divided by the length of the bankfull wetted perimeter. These geometric parameters were surveyed with a hand level and a rod in topographic profiles across channels (Fig. 8). To find the channel bankfull depth h_{bf}, we used gravel bar tops (of height above thalweg z_{bar}), to which we add the water depth critical for the incipient motion of sediment h_c, depth at which $\tau_* = \tau_{*C}$ (Eq. 9), so that $h_{bf} = z_{bar} + h_c$. Channels were identified as fluvial channels by observation of sorting and imbrication of clasts in active channels and incised channel walls (e.g., Miall, 2000, p. 33), and as debris flow–dominated channels by observation of depositional levees, lobes, and snouts (Whipple and Dunne, 1992).

Active faults were identified from satellite imagery and topographic models by their fresh scarps and surface traces (Fig. 5). We checked them against the map of the southern California significant faults from the Southern California Earthquake Data Center (Jennings, 1994) and in the field. The many faults, active and inactive, traverse a fairly complex lithological assemblage ranging from Proterozoic metamorphic rocks to Quaternary volcanic rocks (Jennings, 1958) and demand close-up field inspection to identify the exact location of lithological contacts with respect to waterfalls. We used the 10 m Advanced Spaceborne Thermal Emission and Reflection Radiometer (ASTER) Global Digital Elevation Model (GDEM) V2 (a product of the National Aeronautics and Space Administration [NASA] and Ministry of Economy, Trade, and Industry [METI] of Japan) to survey the alluvial-fan profiles and lengths in Saline, Panamint, and Death Valleys.

All the surveyed streams had bed slopes between 4% and 17% (Fig. 9). To account for this, we chose a morphological drag of 40% ($\tau_m/\tau_T = 0.4$) of the total stress, which corresponds to an average value for steep streams (Scheingross et al., 2013).

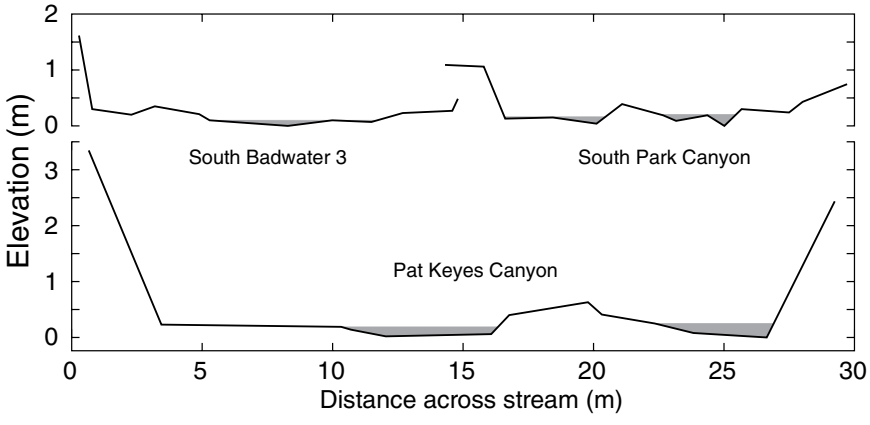

Figure 8. Cross section of three of the surveyed channels where we measured bankfull hydraulic geometry. The bankfull wetted area is represented in gray and is based on the elevation of the top of gravel bars.

RESULTS

Proof of Concept at Gower Gulch

North of the Black Mountains in Death Valley, the Gower Gulch incised active channel has a relatively gentle grade (3.7%, vs. 4.2% for the abandoned channel on the fan surface), and is coarse grained (D_{50} = 16 mm), with a bankfull discharge of Q_w = 27.5 m^3/s (Eq. 6 and Eq. 7) and a total bankfull Shields stress of $\tau_{*T} = 0.36$. We note that τ_{*T} is about six times greater than the critical Shields stress at a slope of ~4% (Lamb et al., 2008). Such a large value corresponds to the range of Shields stresses surveyed on other fans of the region in this study (Table 1) and by Stock et al. (2008).

Unlike the active channel, there are no sediment bars in the steep (4.2%) abandoned channel that could help constrain bankfull hydraulic radius. To remediate this, we use the same bankfull Shield stress calculated for the active channel, and we calculated a bankfull hydraulic radius of R_h = 0.073 m using Equation 9, obtaining a bankfull water discharge of Q_w = 0.8 m^3/s. The measured bed grain sizes in the active channel (D_{50} = 4.2 mm) were a factor of four finer than the active channel. We found that the modern bankfull water discharge was 34-fold the pre-1941 discharge, and this is of the same order as the change in drainage area caused by the engineered diversion (75-fold).

At the Gower Gulch site, we can assess the validity of Equation 1 because we independently know that the difference between the gentle and steep channel-bed slopes is ΔS = 0.5% (from slopes of 3.7% and 4.2%, respectively) and that

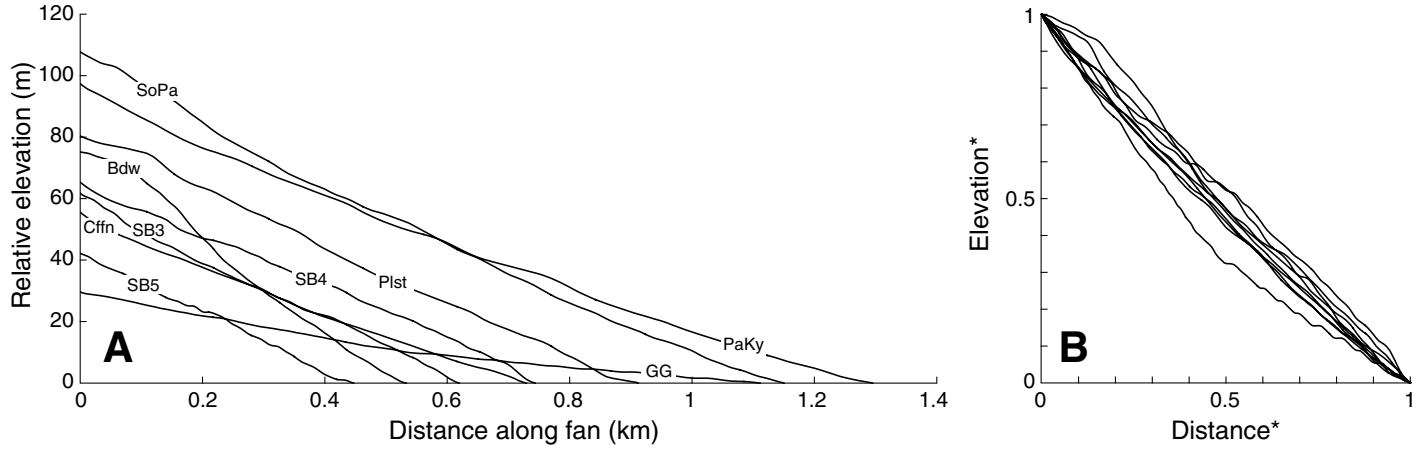

Figure 9. (A) Radial profiles of the alluvial fans of the catchments used to test the fault-burial mechanism. The profiles are approximately linear. Elevation was measured relative to the toe of the fan and was extracted from the 10 m Advanced Spaceborne Thermal Emission and Reflection Radiometer (ASTER) Global Digital Elevation Model (GDEM) V2 (a product of the National Aeronautics and Space Administration [NASA] and Ministry of Economy, Trade, and Industry [METI] of Japan) using GeoMapApp (www.geomapapp.org). Canyon acronyms: GG—Gower Gulch; Bdw—Badwater; SB3, SB4, and SB5—South Badwater 3–5; Cffn—Coffin; Plst—Pleasant; SoPa—South Park; and PaKy—Pat Keyes. (B) Stacked radial profiles normalized by their horizontal and vertical span to highlight their linear slopes.

the height of the waterfall is 6.75 m. Picking a value for the length of the fan is equivocal because its toe is not entirely equidistant to the apex; e.g., Gower Gulch fan is longer on its flanks (1.3 km) than its front (1.1 km; Fig. 6A). We chose to pick the middle section of the fan and measure a length of 1.1 km (dotted line in Fig. 6C). This way, we avoided zones where neighboring fans coalesced, and it was the easiest method to replicate at all sites. Equation 1 predicts a waterfall height of ΔSL_{fan} = 5.5 m. The predicted height is 20% shorter than the measured height of 6.75 m. The difference is partly due to picking a shorter central section for L_{fan}. Alluvial fans often have deposits from debris flows running out at their apexes (Hooke, 1967); this could be another reason why the predicted height somewhat underestimates the actual one. Finally, Equation 1 relies on the assumption of a linear longitudinal profile, and small deviations would cause mismatch between predicted and measured heights (Figs. 6C and 9).

The retreat of knickpoints through the Gower Gulch catchment after the change of hydraulic regime has been documented in Snyder and Kammer (2008). We observed additionally that the fault scarp waterfall lies 4 m in retreat of the fault plane. This corresponds to an upstream waterfall retreat rate of more than 5 cm/yr.

Pleistocene Waterfalls

The 62 surveyed waterfalls have heights ranging from 1 to 25 m and a mean height of 6 ± 4.6 m. The longitudinal profiles of the channels flowing on the alluvial fans (Fig. 9), while slightly concave or convex, satisfactorily match the linear assumption necessary for Equation 1. On all these fans, the active channel is only incised by up to a couple meters at the apex. We evaluated field sites for their application to the fault-burial mechanism based on our field observations. The origins of many other waterfalls have reasonable explanations, and we excluded them from the analysis. Table DR1 (see footnote 1) lists the waterfalls that were kept (19 individual steps) or discarded (43) in the Selection column. The reasoning behind the selection or exclusion is explained below.

The range-bounding faults in both Saline and Death Valley sites have an almost unique surface trace where slip accumulated over multiple cycles of fan aggradation and incision, allowing the repetition of fault burial and exposure. On the contrary, complex surface faulting in Panamint Valley (Fig. 5) is problematic. When the fault splays and creates a new surface rupture at each earthquake, cumulative tectonic displacement cannot build up on one single scarp, and no waterfall greater than the throw of a single earthquake is created. We excluded catchments where field inspection indicated that multiple splay faults close to the waterfalls were recently active (Table DR1 [see footnote 1]).

Our analysis is also restricted to fluvially dominated fans for this study, and we excluded from further analysis fans that we observed to be dominated by debris flows (Table DR1 [see footnote 1]). In Saline Valley, all of the six investigated alluvial fans, except Pat Keyes, were dominated by debris flows. The 13 studied alluvial fans of Panamint and Death Valleys were all dominated by fluvial processes, except for South Badwater 4 in Death Valley. Debris-flow snouts occur at the apex of many fluvially dominated fans in Death Valley, but they do not run out more than at most a few tens of meters on the fan surface (see Hooke, 1967), and the fan channels and exposed stratigraphy are clearly dominated by fluvial deposits.

Close inspection in the field is a necessity to identify and exclude waterfalls that are controlled by lithological contacts or local faults. Lithological contrasts have the potential to allow the development of steep knick zones completely unrelated to the accumulation of tectonic throw on the front fault. For example, in Saline Valley's Craig Canyon, three steep knickpoints higher than 5 m correspond to lumps of a granitic intrusion into a weaker gneissic marble. In Panamint Valley's Surprise Canyon, two successive waterfalls of heights 2.4 and 3.4 m coincide with faults crossing the bedrock channel subparallel to the waterfall plane. The faults are inactive, but there is a systematic contrast of fracture density on either side of the slip plane. The hanging wall is typically densely fractured over a thickness of ~1 m away from the fault plane, while the footwall remains massive. This contrast leads to a differential erodibility that explains the location of the waterfall.

In several streams of Panamint Valley, groups of small waterfalls (between 1 and 5 m) closely succeed each other, and we interpret them as step pools, thus excluding them from analysis. Two particularly high waterfalls (26 and >20 m) were found in South Badwater 3 and 4. Both are the fourth waterfall from the outlet and are at least twice as large as the downstream ones.

TABLE 2. LIST OF ALL THE WATERFALLS SELECTED FOR THE DEMONSTRATION IN SALINE, PANAMINT, AND DEATH VALLEYS

Catchment	Erosion rate (mm/yr)	Uplift (mm/yr)	t_f (yr)	t_u (yr)	t_s (yr)	Heights (m)	Steep slope	Gentle slope	Q_w, modern (m^3/s)	Q_w, past (m^3/s)	Q_w ratio
Gower Gulch, DV	–	–	–	–	–	6.75	0.042	0.037	27.5	0.8	34
Badwater, DV	0.15	2	11,500	4720	9980	9.44	0.131	0.118	0.351	0.371	1.057
S Badwater 3, DV	0.07	2	11,500	6300	8792	12.6	0.089	0.074	0.079	0.101	1.275
S Badwater 3, DV	0.07	2	11,500	3095	4319	[2.03, 4.16]	0.089	0.082	0.079	0.089	1.121
S Badwater 4, DV	0.15	2	11,500	7820	4027	[4.56, 5.55, 5.53]	0.073	0.057	0.104	0.146	1.406
S Badwater 4, DV	0.15	2	11,500	5345	2752	10.69	0.073	0.062	0.104	0.13	1.25
S Badwater 5, DV	0.09	2	11,500	5005	4720	10.01	0.08	0.062	0.29	0.406	1.401
S Badwater 5, DV	0.09	2	11,500	2715	2560	5.43	0.08	0.07	0.29	0.344	1.188
S Badwater 5, DV	0.09	2	11,500	3515	3315	7.03	0.08	0.067	0.29	0.364	1.256
Coffin Canyon, DV	0.06	2	11,500	9300	7328	18.6	0.079	0.06	0.316	0.452	1.43
Pleasant Canyon, PV	0.11	0.34	11,500	4555	3687	8.19	0.053	0.046	0.456	0.479	1.051
South Park Canyon, PV	0.2	0.34	11,500	2365	2239	9.11	0.068	0.061	0.155	0.168	1.09
South Park Canyon, PV	0.2	0.34	11,500	3140	1162	4.73	0.068	0.064	0.155	0.161	1.045
South Park Canyon, PV	0.2	0.34	11,500	4095	1544	6.28	0.068	0.063	0.155	0.164	1.06
Pat Keyes, SV	0.3	0.6	11,500	5830	1538	11.7	0.117	0.111	1.956	2.11	1.079
Pat Keyes, SV	0.3	0.6	11,500	5800	1530	11.6	0.117	0.111	1.956	2.109	1.079

Note: Erosion rates are extrapolated from Kirby (2013). Time scales: t_f—time scale of forcing; t_u—time scale of uplift; t_s—sedimentary time scale. Waterfall heights lumped by a square bracket are in close succession and were considered as one. The maximum t_s was calculated with the volume necessary to aggrade a fan opening at 90° to a height equivalent to the maximum height of the scarp (h_{max}) at the apex, assuming there were no preexisting canyons. DV—Death Valley; PV—Panamint Valley; SV—Saline Valley; Q_w—water discharge.

They are the likely result of several waterfalls that merged during their upstream migration, and we excluded them. Twice, in the canyons of South Badwater 3 and 4, successive steps separated by only a few meters were combined, bringing the number of waterfalls selected for the test from 19 to 15 (Table 2).

Time-Scale Regime

The forcing, uplift, and sedimentary time scales of the selected field sites have to be established to pick a definition of waterfall height (Eqs. 1, 3, or 4) for the analysis. We used a forcing timescale t_f of half of the 23 k.y. precession signal that dominates the recent climatic variability to represent the dry half of the cycle (Table 2). The uplift time scales are easily defined in the Death Valley area, with known, relatively fast fault slip rates (Eq. 2; Table 2). The sedimentary time scale is more difficult to establish. Jayko (2005) provided estimates of denudation rates for the Panamint and Death Valley sites based on the volumes of alluvial fans, assuming that they are entirely built on a flat valley floor. These estimates roughly constrain the coarse fraction of the sediment flux that built the fan, but they underestimate the denudation rate, which includes suspended and dissolved load. In Panamint Valley, Jayko (2005) did not estimate an erosion rate for Pleasant Canyon, and for lack of a better value, we averaged the rates calculated for the two neighboring catchments and obtained 0.11 mm/yr. For the Saline Valley field site, we used denudation rates estimated from ^{10}Be by Kirby (2013), who proposed rates of 0.7–1.2 mm/yr erosion in the steep lower reaches of the Inyo Mountains and 0.05–0.1 mm/yr in the gentler upstream catchment. About 40% of the Pat Keyes catchment is gentle, and 60% is made of steep reaches. Using Kirby's rates, the average denudation rate in this catchment would be 0.6 mm/yr. The ^{10}Be denudation rates describe the entire sediment flux (dissolved, suspended, and bed load), but fans are built with the coarse fraction of the flux only. Without estimates of the different proportions of fluxes, we supposed that the coarse load represents half of the total load at the bottom of these steep catchments, following Turowski et al. (2010). These estimates are sufficient to warrant regime I (Fig. 3); in order to bring any sites into regime III, the erosion rates would have to be at least one order of magnitude lower (Table 2).

Discharge Reconstruction

For each of the 15 waterfalls, we reconstructed the ratio between higher paleoriver water discharge and modern discharge with Equation 13 (Fig. 10). Gower Gulch has a 34-fold increase in water discharge (in this case, pre- and post-1941), while all the other waterfalls point at a mean value of 1.19 ± 0.14 (one standard deviation). The enormous change in water discharge in Gower Gulch did not result in a tall waterfall because the median grain size D concurrently increased from 4.7 mm to 16 mm and limited the decrease in channel slope (Eq. 10). The waterfalls of Panamint and Saline Valley require a smaller change in water discharge ratio (1.07 ± 0.02), while the waterfalls of Death Valley require larger changes in water discharge (1.26 ± 0.13) and display a small positive scaling between discharge ratio and waterfall height.

DISCUSSION

Comparison to Climate Proxies and Uncertainties

Given the important uncertainties affecting estimates of past precipitation levels and in our own reconstructions of absolute water discharge, we cannot require a strict overlap to confirm the validity of the proposed model. Nonetheless we need to evaluate the compatibility of a regional increase of precipitation leading to a 1.19 ± 0.14 rise in water discharge with the climate record. A sediment core in the Badwater Basin of Death Valley indicates significantly wetter conditions from 35 ka to 10 ka while Death Valley hosted the perennial Lake Manly (Lowenstein et al., 1999). A study of the Last Glacial Maximum (LGM) highstand of an endorheic lake in New Mexico suggests doubled LGM precipitation rates in the southwestern United States (Menking et al., 2004). Paleobotanical studies at Yucca Mountain, 85 km NNE of Badwater, propose 1.3–1.4 or 2.1–2.9 times larger precipitations at the LGM (Spaulding, 1985; Thompson et al., 1999, respectively). Finally, an isotopic study of ostracode records in southern Nevada testified to a wetter LGM as well (Quade et al., 2003). The requirement of a 1.19 ± 0.14 greater water discharge for the low channel-bed slope geometry is compatible with all the various climate reconstructions, albeit on the lower end.

Our method requires a series of assumptions affecting the absolute values of the high water discharges that shaped the now-buried gentler channel-bed slope. The main uncertainty in our approach is that we only change the variable Q_w to keep the bankfull Shields stress constant with

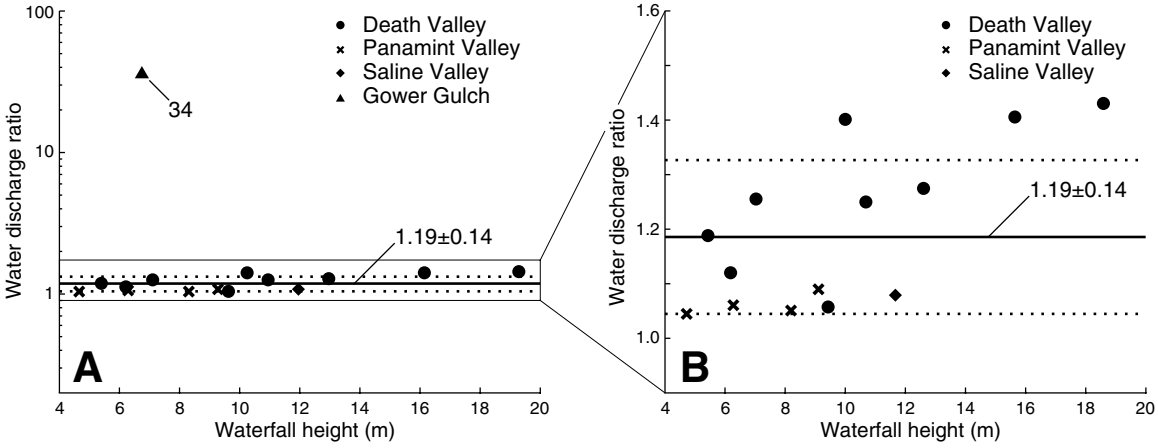

Figure 10. Plot of the ratio between the water discharge controlling the steep slope, calculated from the hydraulic geometry, and the water discharge reconstructed for the gentle slope. (A) Natural sites compared with the case study of Gower Gulch. For the case of Gower Gulch, both water discharges were derived from surveyed hydraulic geometries. (B) Only the natural cases, plotted around the mean value, and the 1σ confidence interval in a linear space.

a changing channel slope, and we ignore the coevolution of Q_s, D, and W. This results in a possible underestimate of the Q_w ratio, since Q_s, D, and W are expected to grow together with Q_w (Gilbert and Murphy, 1914; Leopold and Maddock, 1953; Paola et al., 1992). However, all assumptions were identical for all field sites, and any effect, skewing to greater or smaller values of Q_w, would be equally applied in all our sites. The uniformity of the water discharge ratio across the field sites is important and points at a unique external source of forcing.

Another potential source of error is the assumption that climatic cycles were all similar during the late Pleistocene and Holocene. We used waterfalls presumably created in the late Pleistocene to compute a ratio of water discharges using the modern steep channel slope as a reference for dry conditions. At some sites, we also used multiple successive waterfalls, which, by burial and exposure, would be the products of successive Pleistocene climate cycles. We collapsed all the different episodes onto a single value of water discharge ratio, and for that, we relied on the assumption that Pleistocene climatic cycles were self-similar. The scatter amongst the ratios presented in Figure 10 should be in part explained by variability among climatic cycles during the Pleistocene.

Finally, autogenic dynamics such as landslides, drainage captures, or changes in channel planform morphology can trigger aggradation or incision of the studied alluvial fans, irrespective of climatic forcing. These internally forced events could increase the scatter between sites and/or produce waterfalls unrelated to climate forcing. Such autogenic variations in the modern drainages are unlikely drivers in our study area, as the uniformity among field sites testifies: All fans but one are currently aggraded in a steep geometry.

Further Examples of Fault-Burial Waterfalls

All the field sites of this study lie in a zone of fast active tectonics and are in regime I; that is, we expect waterfalls to reach the height h_{max} (Fig. 3). For the fault-burial mechanism to significantly impact the river system, h_{max} needs to be clearly taller than coseismic throw on the fault. If h_{max} is similar to the coseismic throw, alluvial shielding cannot accumulate displacement greater than the throw of a single event. Its only effect would merely be to delay the release of the coseismic throw in the river system. In Death Valley, h_{max} is as high as 20 m (Fig. 10) and largely exceeds the characteristic coseismic throw of ~2.5 m on the Black Mountain fault (Klinger and Piety, 2001); alluvial shielding can release here the equivalent of two to eight earthquakes in the river system at once.

We expect regime II in areas where the fault throw rates are not fast enough to bring the scarp to the surface. This is the case for Finnegan and Balco's field site in the Santa Lucia Mountains of central California (Finnegan and Balco, 2013). They proposed that Arroyo Seco's alluvial-fan aggradation and incision in Salinas Valley could shield and expose the scarp of the Reliz Canyon fault to release a waterfall in the upstream catchment. However, with a very slow fault throw of 0.015 mm/yr (Rosenberg and Clark, 2005), cyclic aggradation-incision could only result in waterfalls of a height $h_{up} = U \cdot t_f = 0.2$ m, with $t_f = 11.5$ k.y. to represent the wet half of the dominant precession. This height would be a small fraction of h_{max}, which is 30 m according to the current incision of the stream (Finnegan and Balco, 2013). The uplift time scale, t_u, to reach h_{max} is 2 m.y. at the current fault throw rate (Eq. 2). We can also make a rough estimate of the time necessary to fully aggrade the fan, where $t_s = 7.4$ k.y., using Equation 3 and the following parameters. The erosion rate is ~0.1 mm/yr on the eastern slopes of the Santa Lucia Mountains (Griggs and Hein, 1980; Montgomery, 1993), and the area of the Arroyo Seco is ~623 km^2. The volume of the canyon incised in the alluvial fan is ~0.23 km^3, and we set the coarse fraction f_c at 0.5 following Turowski et al. (2010). The Arroyo Seco would squarely sit in regime II ($t_u > t_f > t_s$; Fig. 3). The small knickpoints could nevertheless retreat 12 km in the mudstone bedrock of the lower reach before stalling and accumulating on the crystalline core of the Santa Lucia Mountains, where Finnegan and Balco (2013) documented a large knickpoint that marks the upstream connection of the channel with 30-m-high terraces.

In the Big Tujunga catchment of the San Gabriel Mountains in southern California, DiBiase et al. (2014) proposed that tectonic deformation could accumulate under alluvium before being released as waterfall. The extensive urbanization of the San Gabriel foothills masks the initial geometry of the alluvial fans, and the gentle channel slope of the fan is currently buried. We can nevertheless make an estimate of the volume necessary to aggrade the fan and constrain the sedimentary time scale t_s (Eq. 3). The fan is 7 km long from the Sierra Madre fault zone to the Hansen Dam Flood Protection Basin, with an additional 3 km of backfilling in the valley; the narrow fan is never wider than 700 m;

finally, a change of channel-bed slope of half a percent would result in a shielding thickness of 35 m at the scarp, which defines a total volume of ~8.4 × 10^7 m^3. The ~300 km^2 Big Tujunga catchment erodes at around 0.2 mm/yr (DiBiase et al., 2014), and it would take no more than t_s = 2.8 k.y. to bury the fault scarp entirely (Eq. 3, with k_c = 0.5). The uplift rate is ~1 mm/yr on the Sierra Madre fault zone (Lindvall and Rubin, 2008), and t_f is 35 k.y. if the total burial at the scarp is 35 m. Assuming a climate forcing time scale on a similar period as Death Valley (~11.5 k.y.), the interface between fan and scarp can then produce waterfalls equal to $h = U \cdot t_f$ = 11.5 m. Waterfalls around that height or greater are common in the catchment (DiBiase et al., 2014). The Big Tujunga catchment would lie in regime II with $t_u > t_f > t_s$ (Fig. 3).

Regime III requires a large alluvial fan that aggrades slowly together with a fast fault-slip rate. These conditions go against the trend discussed in Allen and Densmore (2000), which inversely correlates the size of alluvial fans with fault-slip rates, and regime III should rarely be met.

Implications for Landscape Evolution

Alluvial fans can undergo episodes of incision without external forcing caused by feedbacks between the fan and its catchment (Humphrey and Heller, 1995; Carretier and Lucazeau, 2005; Pepin et al., 2010), by changes from sheet to channelized flow (Nicholas and Quine, 2007; van Dijk et al., 2009), or by channel avulsion (Reitz and Jerolmack, 2012). Catchment reorganization by drainage capture will also change the water discharge at the outlet and affect the equilibrium geometry of the alluvial fans of the catchments. The fault-burial mechanism is potentially of great importance for the generation and persistence of autogenic signals in a fan-catchment system that undergoes autogenic incisional phases. As waterfalls retreat in a drainage basin, they force a local pulse of erosion by immediately lowering the hillslope base level (Gallen et al., 2011; Attal et al., 2015). In turn, this erosion pulse will increase the ratio Q_s/Q_w and could lead to aggradation of the fan and renewed shielding of an active scarp until the erosion pulse initiated by the waterfall propagates through the entire catchment. This dynamic is a potential driver to help sustain a series of feedbacks between fan and catchment that would lead the fan to an oscillation between periods of net aggradation and deposition called "tintinnabulation" by Humphrey and Heller (1995). As a result, the landscape is constantly reacting to new internal adjustments that do not reflect changes in its environment.

Feedbacks in a coupled catchment-fan system are further illustrated in Figure 11. Consider a system in regime I forced by a cyclic climate with alternation of wet and dry phases and regular earthquakes that force base-level fall (Fig. 11B). The alluvial fan aggrades in dry periods and incises during wet ones, alternatively burying and exposing the active fault scarp (Fig. 11C). Meanwhile, the fault ruptures repeatedly, and coseismic waterfalls are released in the river in the absence of an alluvial shield, or tectonic slip accumulates until bedrock pierces through alluvium when alluvial fill buries the scarp (Fig. 11C, using the same representation introduced in Fig. 11A). Tectonic throw reaches the new base level during the period of shielding. At the end of this period, the fan incises back to a gentle configuration, and

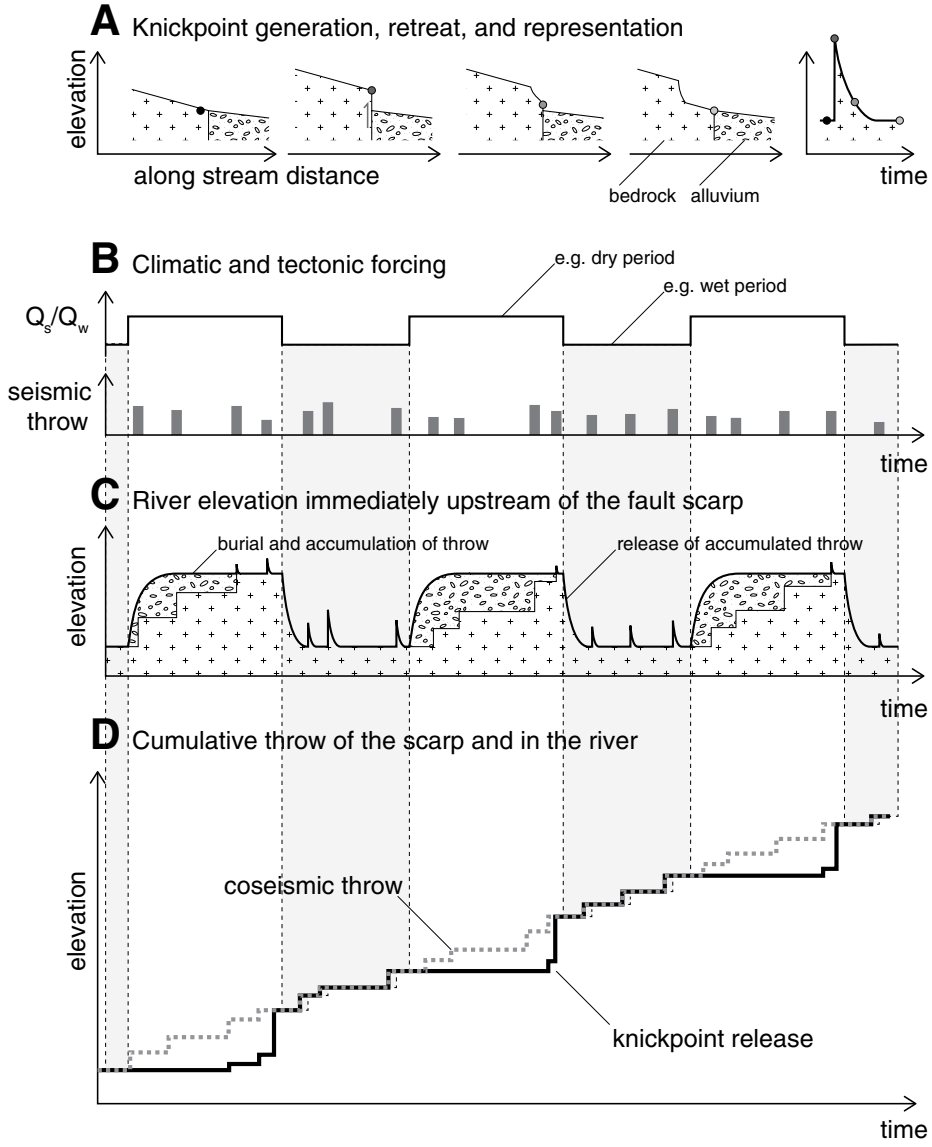

Figure 11. Effect of the regime I fault-burial mechanism on knickpoint release in the river system. (A) The creation of a coseismic knickpoint and subsequent retreat upstream can be represented as the elevation of the stream immediately upstream of the scarp. (B) Periodic climatic forcing expressed as the ratio between sediment flux and water discharge, and tectonic forcing represented by the throw of earthquakes on the range-bounding fault. (C) The elevation of the riverbed immediately upstream of the fault scarp (using the representation introduced in A) shows how the tectonic and climatic forcing in B are translated into alluvial aggradation and uplift of the scarp. (D) The cumulative release of waterfalls in the river system differs from the coseismic throw due to burial and incision.

the total accumulated throw h_{max} is released as a large knickpoint in the river system (Fig. 11C). The climate-governed alluvial fan thus acts as a filter on the tectonic forcing, releasing seismic throw in rarer and bigger steps on a climatic beat (dotted vs. solid line in Fig. 11D).

The processes controlling waterfall retreat are not yet understood, and it is not clear whether and how waterfall retreat rate scales with waterfall height. Hayakawa and Matsukura (2003) proposed that waterfall retreat rate scales negatively with waterfall height because the erosive force of the stream would be distributed over a greater area for larger waterfalls. In that case, releasing fewer, larger, and more slowly retreating waterfalls would augment the response time of a catchment. However, Whittaker and Boulton (2012) showed that knickpoints retreat faster in regions of greater uplift. They proposed that large-amplitude tectonic perturbations result in shorter landscape response times. Although waterfalls cannot be directly compared with the knickpoints of Whittaker and Boulton (2012), the relationship between faster retreat rates and greater disturbances along the river profile could hold for single waterfalls and very steep knick zones. Additionally, if all or part of the retreat of a waterfall results from the impact of sediments on canyon walls during free fall, then higher waterfalls should result in more energetic impacts, and the retreat rate could scale positively with waterfall height (Lamb and Dietrich, 2009; Scheingross et al., 2017). Faster retreat rates for larger waterfalls would suggest that the discrete release of accumulated slip shortens the landscape reaction time and enhances its reactivity (Allen, 2005). As these knickpoints are exposed according to a climatic beat, they have the capacity to reduce the damping of climate-driven sediment fluxes (Armitage et al., 2013). In consequence, the fault-burial mechanism has the potential to improve the sensitivity of the sedimentary record to higher-frequency cycles (Simpson and Castelltort, 2012).

CONCLUSION

We demonstrate that waterfalls can be created over an intermittently alluviated dip-slip fault. Burial of the fault scarp by sediments during periods of alluvial aggradation allows the accumulation of tectonic slip and its sudden release during subsequent incision. We established three time scales controlling the generation of waterfalls: forcing, uplift, and sedimentary time scales. The relative durations of these time scales define three regimes in which waterfall height can be calculated with analytical solutions. The maximum height of a waterfall produced by fault burial depends on the length of the alluvial fan and on the gentle and steep bedslope configurations of its channel.

We tested and validated the fault-burial mechanism against a fully constrained, man-made episode of alluvial-fan incision driven by a 75-fold change in drainage area in Gower Gulch (Death Valley, California), which led to the uncovering of a 6.75 m waterfall at the active fault scarp. We showed that the fault-burial mechanism can relate otherwise unexplained waterfalls of 4–19 m in the Death Valley area to ~20% variations in precipitations during the late Pleistocene and Holocene. The wet-dry climate cycles led to the aggradation and incision necessary for the fault-burial mechanism. The fault-burial mechanism is relevant wherever surface tectonic deformation is intermittently covered by sediments. Through the modulation of waterfall heights, the fault-burial mechanism can affect the response time of a landscape to downstream forcing by changing the retreat rate of knickpoints. Waterfalls created this way by climate-driven aggradation and incision convolve tectonic and climatic signals.

ACKNOWLEDGMENTS

We thank Austin Chadwick, Alistair Hayden, Marisa Palucis, and Victoria Stevens for support in the field, and Mitch D'Arcy and Roman DiBiase for fruitful discussions. We thank S. Boulton and an anonymous reviewer as well as Associate Editor Karl Wegmann for their helpful reviews. This work was supported by a Doc. Mobility Fellowship of the Swiss National Science Foundation (project number: P1SKP2 158716) to L.C. Malatesta; National Science Foundation grant 1147381 to M.P. Lamb; and acknowledgment is made to the Donors of the American Chemical Society Petroleum Research Fund for partial support of this research (grant 53204-ND8). Field work in the Death Valley National Park is registered as study DEVA-00409 with permit DEVA-2014-SCI-0040.

REFERENCES CITED

Allen, P.A., 2005, Striking a chord: Nature, v. 434, p. 961, doi:10.1038/434961a.

Allen, P.A., and Densmore, A.L., 2000, Sediment flux from an uplifting fault block: Basin Research, v. 12, p. 367–380, doi:10.1046/j.1365-2117.2000.00135.x.

Armitage, J.J., Dunkley Jones, T., Duller, R.A., Whittaker, A.C., and Allen, P.A., 2013, Temporal buffering of climate-driven sediment flux cycles by transient catchment response: Earth and Planetary Science Letters, v. 369–370, p. 200–210, doi:10.1016/j.epsl.2013.03.020.

Attal, M., Mudd, S.M., Hurst, M.D., Weinman, B., Yoo, K., and Naylor, M., 2015, Impact of change in erosion rate and landscape steepness on hillslope and fluvial sediments grain size in the Feather River basin (Sierra Nevada, California): Earth Surface Dynamics, v. 3, p. 201–222, doi:10.5194/esurf-3-201-2015.

Berlin, M.M., and Anderson, R.S., 2007, Modeling of knickpoint retreat on the Roan Plateau, western Colorado: Journal of Geophysical Research–Earth Surface, v. 112, F03S06, doi:10.1029/2006JF000553.

Bishop, P., Hoey, T.B., Jansen, J.D., and Artza, I.L., 2005, Knickpoint recession rate and catchment area: The case of uplifted rivers in eastern Scotland: Earth Surface Processes and Landforms, v. 30, p. 767–778, doi:10.1002/esp.1191.

Bull, W.B., 1964, Geomorphology of Segmented Alluvial Fans in Western Fresno County, California: U.S. Geological Survey Professional Paper 352, p. 89–129.

Bull, W.B., 1991, Geomorphic Responses to Climatic Change: New York, Oxford University Press, 326 p.

Burchfiel, B.C., Hodges, K.V., and Royden, L.H., 1987, Geology of Panamint Valley–Saline Valley Pull-Apart System, California: Palinspastic evidence for low-angle geometry of a Neogene range-bounding fault: Journal of Geophysical Research–Earth Surface, v. 92, p. 10,422–10,426, doi:10.1029/JB092iB10p10422.

Carretier, S., and Lucazeau, F., 2005, How does alluvial sedimentation at range fronts modify the erosional dynamics of mountain catchments?: Basin Research, v. 17, p. 361–381, doi:10.1111/j.1365-2117.2005.00270.x.

Chatanantavet, P., and Parker, G., 2009, Physically based modeling of bedrock incision by abrasion, plucking, and macroabrasion: Journal of Geophysical Research–Solid Earth, v. 114, F04018, doi:10.1029/2008JF001044.

Chen, Y.-G., Chen, W.-S., Wang, Y., Lo, P.-W., Liu, T.-K., and Lee, J.-C., 2002, Geomorphic evidence for prior earthquakes: Lessons from the 1999 Chichi earthquake in central Taiwan: Geology, v. 30, p. 171–174, doi:10.1130/0091-7613(2002)030<0171:GEFPEL>2.0.CO;2.

Clark, M.K., Maheo, G., Saleeby, J., and Farley, K.A., 2005, The non-equilibrium landscape of the southern Sierra Nevada, California: GSA Today, v. 15, no. 9, p. 4–10, doi:10:1130/1052–5173(2005)015<4:TNELOT>2.0.CO;2.

Cook, K.L., Whipple, K.X., Heimsath, A.M., and Hanks, T.C., 2009, Rapid incision of the Colorado River in Glen Canyon—Insights from channel profiles, local incision rates, and modeling of lithologic controls: Earth Surface Processes and Landforms, v. 34, p. 994–1010, doi:10.1002/esp.1790.

Cook, K.L., Turowski, J.M., and Hovius, N., 2013, A demonstration of the importance of bedload transport for fluvial bedrock erosion and knickpoint propagation: Earth Surface Processes and Landforms, v. 38, p. 683–695, doi:10.1002/esp.3313.

Crosby, B.T., and Whipple, K.X., 2006, Knickpoint initiation and distribution within fluvial networks: 236 waterfalls in the Waipaoa River, North Island, New Zealand: Geomorphology, v. 82, p. 16–38, doi:10.1016/j.geomorph.2005.08.023.

D'Arcy, M., Roda Boluda, D.C., Whittaker, A.C., and Carpineti, A., 2014, Dating alluvial fan surfaces in Owens Valley, California, using weathering fractures in boulders: Earth Surface Processes and Landforms, v. 40, p. 487–501, doi:10.1002/esp.3649.

D'Arcy, M., Whittaker, A.C., and Roda Boluda, D.C., 2016, Measuring alluvial fan sensitivity to past climate changes using a self-similarity approach to grain size fining, Death Valley, California: Sedimentology, v. 64, no. 2, p. 388–424, doi:10.1111/sed.12308.

DeLong, S.B., Pelletier, J.D., and Arnold, L.J., 2008, Climate change triggered sedimentation and progressive tectonic uplift in a coupled piedmont–axial system: Cuyama Valley, California, USA: Earth Surface Processes and Landforms, v. 33, p. 1033–1046, doi:10.1002/esp.1600.

Densmore, A.L., Allen, P.A., and Simpson, G., 2007, Development and response of a coupled catchment fan system under changing tectonic and climatic forcing: Journal of Geophysical Research–Solid Earth, v. 112, F01002, doi:10.1029/2006JF000474.

DiBiase, R.A., Whipple, K.X., Lamb, M.P., and Heimsath, A.M., 2014, The role of waterfalls and knickzones in controlling the style and pace of landscape adjustment in the western San Gabriel Mountains, California: Geological Society of America Bulletin, v. 127, p. 539–559, doi:10.1130/B31113.1.

Dzurisin, D., 1975, Channel responses to artificial stream capture, Death Valley, California: Geology, v. 3, p. 309–312, doi:10.1130/0091-7613(1975)3<309:CRTASC>2.0.CO;2.

Einstein, H.A., and Barbarossa, N.L., 1952, River channel roughness: Transactions of the American Society of Civil Engineers, v. 117, p. 1121–1132.

Finnegan, N.J., and Balco, G., 2013, Sediment supply, base level, braiding, and bedrock river terrace formation:

Arroyo Seco, California, USA: Geological Society of America Bulletin, v. 125, p. 1114–1124, doi:10.1130/B30727.1.

Frankel, K.L., Pazzaglia, F.J., and Vaughn, J.D., 2007, Knickpoint evolution in a vertically bedded substrate, upstream-dipping terraces, and Atlantic slope bedrock channels: Geological Society of America Bulletin, v. 119, p. 476–486, doi:10.1130/B25965.1.

Frankel, K.L., Glazner, A.F., Kirby, E., Monastero, F.C., Strane, M.D., Oskin, M.E., Unruh, J.R., Walker, J.D., Anandakrishnan, S., Bartley, J.M., Coleman, D.S., Dolan, J.F., Finkel, R.C., Greene, D., et al., 2008, Active tectonics of the Eastern California shear zone, *in* Duebendorfer, E.M., and Smith, E.I., eds., Field Guide to Plutons, Volcanoes, Faults, Reefs, Dinosaurs, and Possible Glaciation in Selected Areas of Arizona, California, and Nevada: Geological Society of America Field Guide 11, p. 43–81.

Frankel, K.L., Owen, L.A., Dolan, J.F., Knott, J.R., Lifton, Z.M., Finkel, R.C., and Wasklewicz, T., 2015, Timing and rates of Holocene normal faulting along the Black Mountains fault zone, Death Valley, USA: Lithosphere, v. 8, p. 3–22, doi:10.1130/L464.1.

Freeze, R.A., 1974, Streamflow generation: Reviews of Geophysics, v. 12, p. 627–647, doi:10.1029/RG012i004p00627.

Gallen, S.F., Wegmann, K.W., Frankel, K.L., Hughes, S., Lewis, R.Q., Lyons, N., Paris, P., Ross, K., Bauer, J.B., and Witt, A.C., 2011, Hillslope response to knickpoint migration in the Southern Appalachians: Implications for the evolution of post-orogenic landscapes: Earth Surface Processes and Landforms, v. 36, p. 1254–1267, doi:10.1002/esp.2150.

Gilbert, G.K., and Murphy, E.C., 1914, The Transportation of Debris by Running Water: U.S. Geological Survey Professional Paper 86, 263 p.

Griggs, G.B., and Hein, J.R., 1980, Sources, dispersal, and clay mineral composition of fine-grained sediment off central and northern California: The Journal of Geology, v. 88, p. 541–566, doi:10.1086/628543.

Hart, E.W., Bryant, W.A., Wills, C.J., Treiman, J.A., and Kahle, J.E., 1989, Summary Report: Fault Evaluation Program, 1987–1988, Southwestern Basin and Range Region and Supplemental Areas: California Department of Conservation, Division of Mines and Geology, Bay Area Regional Office, Open-File Report 89-16, 31 p.

Harvey, A.M., Wigand, P.E., and Wells, S.G., 1999, Response of alluvial fan systems to the late Pleistocene to Holocene climatic transition: Contrasts between the margins of pluvial Lakes Lahontan and Mojave, Nevada and California, USA: Catena, v. 36, p. 255–281, doi:10.1016/S0341-8162(99)00049-1.

Hayakawa, Y., and Matsukura, Y., 2003, Recession rates of waterfalls in Boso Peninsula, Japan, and a predictive equation: Earth Surface Processes and Landforms, v. 28, p. 675–684, doi:10.1002/esp.519.

Hooke, R.L., 1967, Processes on arid-region alluvial fans: The Journal of Geology, v. 75, p. 438–460, doi:10.1086/627271.

Hooke, R.L., 1968, Steady-state relationships on arid-region alluvial fans in closed basins: American Journal of Science, v. 266, p. 609–629, doi:10.2475/ajs.266.8.609.

Horton, R.E., 1945, Erosional development of streams and their drainage basins; hydrophysical approach to quantitative morphology: Geological Society of America Bulletin, v. 56, p. 275–370, doi:10.1130/0016-7606(1945)56[275:EDOSAT]2.0.CO;2.

Howard, A.D., 1994, A detachment-limited model of drainage basin evolution: Water Resources Research, v. 30, p. 2261–2285, doi:10.1029/94WR00757.

Huang, M.-W., Pan, Y.-W., and Liao, J.-J., 2013, A case of rapid rock riverbed incision in a coseismic uplift reach and its implications: Geomorphology, v. 184, p. 98–110, doi:10.1016/j.geomorph.2012.11.022.

Humphrey, N.F., and Heller, P.L., 1995, Natural oscillations in coupled geomorphic systems—An alternative origin for cyclic sedimentation: Geology, v. 23, p. 499–502, doi:10.1130/0091-7613(1995)023<0499:NOICGS>2.3.CO;2.

Jayko, A.S., 2005, Late Quaternary denudation, Death and Panamint Valleys, eastern California: Earth-Science Reviews, v. 73, p. 271–289, doi:10.1016/j.earscirev.2005.04.009.

Jennings, C.W., 1958, Geologic Map of California: Death Valley Sheet: Sacramento, California Division of Mines and Geology, scale 1:250,000.

Jennings, C.W., 1994, Fault Activity Map of California and Adjacent Areas with Location and Ages of Recent Volcanic Eruptions: California Division of Mines and Geology California Geologic Data Map Series Map 6, scale 1:750,000.

Kirby, E., 2013, Reading the signal of tectonics in landscape topography: Challenges and opportunities, *in* European Geosciences Union General Assembly: Vienna, Austria, abstract EGU2013-11963.

Klinger, R.E., and Piety, L.A., 2001, Holocene faulting and slip rates along the Black Mountains fault zone near Mormon Point, *in* Machette, M.N., Johnson, M.L., and Slate, J.L. eds., Quaternary and Late Pliocene Geology of the Death Valley Region: Recent Observations on Tectonics, Stratigraphy, and Lake Cycles (Guidebook for the 2001 Pacific Cell—Friends of the Pleistocene Fieldtrip): U.S. Geological Survey Open-File Report 01-51, p. L193–L203.

Knox, J.C., 1975, Concept of the graded stream, *in* Melhorn, W.N., and Flemal, R.C., eds., Theories of Landform Development, Theories of Landform Development: London, State University of New York, p. 169–198.

Ku, T.-L., Luo, S., Lowenstein, T.K., Li, J., and Spencer, R.J., 1998, U-series chronology of lacustrine deposits in Death Valley, California: Quaternary Research, v. 50, p. 261–275, doi:10.1006/qres.1998.1995.

Lamb, M.P., and Dietrich, W.E., 2009, The persistence of waterfalls in fractured rock: Geological Society of America Bulletin, v. 121, p. 1123–1134, doi:10.1130/B26482.1.

Lamb, M.P., Howard, A.D., Dietrich, W.E., and Perron, J.T., 2007, Formation of amphitheater-headed valleys by waterfall erosion after large-scale slumping on Hawai'i: Geological Society of America Bulletin, v. 119, p. 805–822, doi:10.1130/B25986.1.

Lamb, M.P., Dietrich, W.E., and Venditti, J.G., 2008, Is the critical Shields stress for incipient sediment motion dependent on channel-bed slope?: Journal of Geophysical Research, v. 113, F02008, doi:10.1029/2007JF000831.

Lamb, M.P., Scheingross, J.S., Amidon, W.H., Swanson, E., and Limaye, A., 2011, A model for fire-induced sediment yield by dry ravel in steep landscapes: Journal of Geophysical Research–Solid Earth, v. 116, F03006, doi:10.1029/2010JF001878.

Lane, E.W., 1937, Stable channels in erodible material: Transactions of the American Society of Civil Engineers, v. 102, p. 123–142.

Lane, E.W., 1955, Design of stable channels: Transactions of the American Society of Civil Engineers, v. 120, p. 1234–1279.

Lee, J., Stockli, D.F., Owen, L.A., Finkel, R.C., and Kislitsyn, R., 2009, Exhumation of the Inyo Mountains, California: Implications for the timing of extension along the western boundary of the Basin and Range Province and distribution of dextral fault slip rates across the Eastern California shear zone: Tectonics, v. 28, TC1001, doi:10.1029/2008TC002295.

Lee, Y.H., Lu, S.-T., Hsieh, M.-L., and Wu, W.-Y., 2005, Structures associated with the northern end of the 1999 Chi-Chi earthquake rupture, central Taiwan: Implications for seismic-hazard assessment: Bulletin of the Seismological Society of America, v. 95, p. 471–485, doi:10.1785/0120020170.

Leopold, L.B., and Bull, W.B., 1979, Base level, aggradation, and grade: Proceedings of the American Philosophical Society, v. 123-3, p. 168–202.

Leopold, L.B., and Maddock, T., Jr., 1953, The Hydraulic Geometry of Stream Channels and Some Physiographic Implications: U.S. Geological Survey Professional Paper 252, 57 p.

Lindvall, S.C., and Rubin, C.M., 2008, Slip Rate Studies Along the Sierra Madre–Cucamonga Fault System Using Geomorphic and Cosmogenic Surface Exposure Age Constraints: Collaborative Research with Central Washington University and William Lettis & Associates, Inc.: U.S. Geological Survey Final Report 03HQGR0084, p. 1–13.

Lowenstein, T.K., Li, J., Brown, C., Roberts, S.M., Ku, T.-L., Luo, S., and Yang, W., 1999, 200 k.y. paleoclimate record from Death Valley salt core: Geology, v. 27, p. 3–6, doi:10.1130/0091-7613(1999)027<0003:KYPRFD>2.3.CO;2.

Mackey, B.H., Scheingross, J.S., Lamb, M.P., and Farley, K.A., 2014, Knickpoint formation, rapid propagation, and landscape response following coastal cliff retreat at the last interglacial sea-level highstand: Kaua'i, Hawai'i: Geological Society of America Bulletin, v. 126, p. 925–942, doi:10.1130/B30930.1.

Mackin, J.H., 1948, Concept of the graded river: Geological Society of America Bulletin, v. 59, p. 463–511, doi:10.1130/0016-7606(1948)59[463:COTGR]2.0.CO;2.

Mason, C.C., and Romans, B.W., 2015, Quantifying sediment supply in stratigraphy using cosmogenic nuclides: Insights from the Pleasant Canyon complex, Panamint Mountains, California, *in* American Association of Petroleum Geologists Annual Convention and Exhibition: Boulder, Colorado, American Association of Petroleum Geologists Article 90216.

Menking, K.M., Anderson, R.Y., Shafike, N.G., Syed, K.H., and Allen, B.D., 2004, Wetter or colder during the Last Glacial Maximum? Revisiting the pluvial lake question in southwestern North America: Quaternary Research, v. 62, p. 280–288, doi:10.1016/j.yqres.2004.07.005.

Meyer-Peter, E., and Müller, R., 1948, Formulas for bed-load transport, *in* 2nd Meeting of the International Association for Hydraulic Structures Research: Stockholm, Sweden, International Association for Hydraulic Structures Research, p. 39–64.

Miall, A.D., 2000, Principles of Sedimentary Basin Analysis (3rd ed.): Heidelberg, Germany, Springer, 616 p., doi:10.1007/978-3-662-03999-1.

Montgomery, D.R., 1993, Compressional uplift in the central California Coast Ranges: Geology, v. 21, p. 543–546, doi:10.1130/0091-7613(1993)021<0543:CUITCC>2.3.CO;2.

Nicholas, A.P., and Quine, T.A., 2007, Modeling alluvial landform change in the absence of external environmental forcing: Geology, v. 35, p. 527–530, doi:10.1130/G23377A.1.

Numelin, T., Marone, C., and Kirby, E., 2007, Frictional properties of natural fault gouge from a low-angle normal fault, Panamint Valley, California: Tectonics, v. 26, TC2004, doi:10.1029/2005TC001916.

Paola, C., Heller, P.L., and Angevine, C.L., 1992, The large-scale dynamics of grain-size variation in alluvial basins: 1. Theory: Basin Research, v. 4, p. 73–90, doi:10.1111/j.1365-2117.1992.tb00145.x.

Parker, G., 1978, Self-formed straight rivers with equilibrium banks and mobile bed. Part 2. The gravel river: Journal of Fluid Mechanics, v. 89, p. 127–146, doi:10.1017/S0022112078002505.

Parker, G., 1991, Selective sorting and abrasion of river gravel. 2. Applications: Journal of Hydraulic Engineering, v. 117, p. 150–171, doi:10.1061/(ASCE)0733-9429(1991)117:2(150).

Parker, G., Paola, C., Whipple, K.X., and Mohrig, D., 1998, Alluvial fans formed by channelized fluvial and sheet flow: I. Theory: Journal of Hydraulic Engineering, v. 124, p. 985–995, doi:10.1061/(ASCE)0733-9429(1998)124:10(985).

Parker, G., Wilcock, P.R., Paola, C., Dietrich, W.E., and Pitlick, J., 2007, Physical basis for quasi-universal relations describing bankfull hydraulic geometry of single-thread gravel bed rivers: Journal of Geophysical Research, v. 112, F04005, doi:10.1029/2006JF000549.

Pepin, E., Carretier, S., and Herail, G., 2010, Erosion dynamics modelling in a coupled catchment-fan system with constant external forcing: Geomorphology, v. 122, p. 78–90, doi:10.1016/j.geomorph.2010.04.029.

Poisson, B., and Avouac, J.-P., 2004, Holocene hydrological changes inferred from alluvial stream entrenchment in North Tian Shan (northwestern China): The Journal of Geology, v. 112, p. 231–249, doi:10.1086/381659.

Quade, J., Forester, R.M., and Whelan, J.F., 2003, Late Quaternary paleohydrologic and paleotemperature change in southern Nevada, *in* Enzel, Y., Wells, S.G., and Lancaster, N., eds., Paleoenvironments and Paleohydrology of the Mojave and Southern Great Basin Deserts: Geological Society of America Special Paper 368, p. 165–188, doi:10.1130/0-8137-2368-X.165.

Reitz, M.D., and Jerolmack, D.J., 2012, Experimental alluvial fan evolution: Channel dynamics, slope

controls, and shoreline growth: Journal of Geophysical Research–Solid Earth, v. 117, p. 1–19, doi:10.1029/2011JF002261.

Rohais, S., Bonnet, S., and Eschard, R., 2012, Sedimentary record of tectonic and climatic erosional perturbations in an experimental coupled catchment-fan system: Basin Research, v. 24, p. 198–212, doi:10.1111/j.1365-2117.2011.00520.x.

Rosenberg, L.I., and Clark, J.C., 2005, Neotectonics of the Rinconada and Reliz fault zones, Salinas Valley, California: Geological Society of America Abstracts with Programs, v. 37, no. 4, p. 106.

Scheingross, J.S., Winchell, E.W., Lamb, M.P., and Dietrich, W.E., 2013, Influence of bed patchiness, slope, grain hiding, and form drag on gravel mobilization in very steep streams: Journal of Geophysical Research–Earth Surface, v. 118, p. 982–1001, doi:10.1002/jgrf.20067.

Scheingross, J.S., Lo, D.Y., and Lamb, M.P., 2017, Self-formed waterfall plunge pools in homogeneous rock: Geophysical Research Letters, v. 44, p. 200–208, doi:10.1002/2016GL071730.

Schumm, S.A., 1973, Geomorphic thresholds and complex response of drainage systems, *in* Morisawa, M., ed., Fluvial Geomorphology, Fourth Annual Geomorphology Symposia Series: New York, Binghamton, State University of New York, p. 299–310.

Simpson, G., and Castelltort, S., 2012, Model shows that rivers transmit high-frequency climate cycles to the sedimentary record: Geology, v. 40, p. 1131–1134, doi:10.1130/G33451.1.

Sklar, L.S., and Dietrich, W.E., 2004, A mechanistic model for river incision into bedrock by saltating bed load: Water Resources Research, v. 40, p. 1–21, doi:10.1029/2003WR002496.

Snyder, N.P., and Kammer, L.L., 2008, Dynamic adjustments in channel width in response to a forced diversion: Gower Gulch, Death Valley National Park, California: Geology, v. 36, p. 187–190, doi:10.1130/G24217A.1.

Spaulding, W.G., 1985, Vegetation and Climates of the last 45,000 Years in the Vicinity of the Nevada Test Site, South-Central Nevada: U.S. Geological Service Professional Paper 1329, 90 p.

Stock, J.D., Schmidt, K.M., and Miller, D.M., 2008, Controls on alluvial fan long-profiles: Geological Society of America Bulletin, v. 120, p. 619–640, doi:10.1130/B26208.1.

Thompson, R.S., Anderson, K.H., and Bartlein, P.J., 1999, Quantitative Paleoclimatic Reconstructions from Late Pleistocene Plant Macrofossils of the Yucca Mountain Region: U.S. Geological Service Open-File Report 99-338, 39 p.

Trampush, S.M., Huzurbazar, S., and McElroy, B., 2014, Empirical assessment of theory for bankfull characteristics of alluvial channels: Water Resources Research, v. 50, p. 9211–9220, doi:10.1002/2014WR015597.

Troxel, B.W., 1974, Man-made diversion of Furnace Creek Wash, Zabriskie Point, Death Valley, California: California Geology, v. 27, p. 219–223.

Turowski, J.M., Rickenmann, D., and Dadson, S.J., 2010, The partitioning of the total sediment load of a river into suspended load and bedload: A review of empirical data: Sedimentology, v. 57, p. 1126–1146, doi:10.1111/j.1365-3091.2009.01140.x.

van Dijk, M., Postma, G., and Kleinhans, M.G., 2009, Autocyclic behaviour of fan deltas: An analogue experimental study: Sedimentology, v. 56, p. 1569–1589, doi:10.1111/j.1365-3091.2008.01047.x.

Vogel, M.B., Jayko, A.S., Wooden, J.L., and Smith, R.S.U., 2002, Quaternary exhumation rate central Panamint Range, California, from U-Pb zircon ages: Denver, Geological Society of American Abstracts with Programs, paper no. 111-9.

Wells, S.G., and Harvey, A.M., 1987, Sedimentologic and geomorphic variations in storm-generated alluvial fans, Howgill Fells, northwest England: Geological Society of America Bulletin, v. 98, p. 182–198, doi:10.1130/0016-7606(1987)98<182:SAGVIS>2.0.CO;2.

Whipple, K.X., and Dunne, T., 1992, The influence of debris-flow rheology on fan morphology, Owens Valley, California: Geological Society of America Bulletin, v. 104, p. 887–900, doi:10.1130/0016-7606(1992)104<0887:TIODFR>2.3.CO;2.

Whipple, K.X., and Trayler, C.R., 1996, Tectonic control of fan size: The importance of spatially variable subsidence rates: Basin Research, v. 8, p. 351–366, doi:10.1046/j.1365-2117.1996.00129.x.

Whipple, K.X., DiBiase, R.A., and Crosby, B.T., 2013, Bedrock rivers, *in* Shroder, J., Jr., and Wohl, E., eds., Treatise on Geomorphology, Volume 9: Amsterdam, Netherlands, Elsevier, p. 550–573.

Whittaker, A.C., and Boulton, S.J., 2012, Tectonic and climatic controls on knickpoint retreat rates and landscape response times: Journal of Geophysical Research–Solid Earth, v. 117, F02024, doi:10.1029/2011JF002157.

Wobus, C., Whipple, K.X., Kirby, E., Snyder, N., Johnson, J., Spyropolou, K., Crosby, B., and Sheehan, D., 2006, Tectonics from topography: Procedures, promise, and pitfalls, *in* Willett, S., Hovius, N., Brandon, M.T., and Fisher, D.M., eds., Tectonics, Climate, and Landscape Evolution: Geological Society of America Special Paper 398, p. 55–74, doi:10.1130/2006.2398(04).

Wong, M., and Parker, G., 2006, Reanalysis and correction of bed-load relation of Meyer-Peter and Muller using their own database: Journal of Hydraulic Engineering, v. 132, p. 1159–1168, doi:10.1061/(ASCE)0733-9429(2006)132:11(1159).

Science Editor: Bradley S. Singer
Associate Editor: Karl W. Wegmann

Manuscript Received 9 January 2017
Revised Manuscript Received 28 June 2017
Manuscript Accepted 11 August 2017

Printed in the USA